Study on the Design of Soft Surgical Robots for Endoscopic NOTES Applications

M.W. (Muhammad) Gifari

MSc Report

Committee:
Prof.dr.ir. C.H. Slump
Dr.ir. M. Abayazid
H. Naghibi Beidokhti, MSc
Dr. L. Masia

August 2018

031RAM2018
Robotics and Mechatronics
EE-Math-CS
University of Twente
P.O. Box 217
7500 AE Enschede
The Netherlands

UNIVERSITY OF TWENTE.

MIRA CTIT
BIOMEDICAL TECHNOLOGY AND TECHNICAL MEDICINE

Summary

With the advance of surgical operation from open surgery toward Minimally Invasive Surgery (MIS) and recently Natural Orifice Transluminal Endoscopic Surgery (NOTES) the surgeons are barely keeping up with the instrumentation. Endoscope that was originally a tool to examine the inside of patient body is now developed to perform surgical task. Advances have been made in the conventional endoscopic instruments, however several problems still arise.

The conventional endoscopic instruments can be categorized into two categories: rigid and flexible instrument. When the target organ is near incision point, such as in MIS, surgeons will place trocar and insert rigid endoscopes (can be several endoscopes at once) to perform the surgery. While this tool provide stability, it does not have flexibility. This rigid instrument is only effective when the target organ is directly in front of the incision point. When the target organ is deep inside patient body, or obscured by other organ, such as in gastrointestinal (GI) surgery, then flexible endoscope is the choice. Clearly this endoscope allows flexible navigation inside patient lumen. However, when a surgical intervention is performed, this flexible endoscope is not stable enough to perform the required operation.

Other problem of flexible endoscope is the trackability of the instrument inside the patient lumen. In case of rigid endoscope, trackability is not an issue because the instrument is not deeply inserted. In case of flexible endoscope, the view of endoscopic camera is usually narrow and currently the endoscope is not trackable inside the lumen. The endoscope may end up in wrong branch or arriving at incorrect operation target. Another limitation of flexible endoscope is the control method. Currently, the surgeons push the instrument manually inside patient body, and control is possible only at the tip of endoscope. This may cause the endoscope to form a loop inside patient body. In this case, further pushing of the endoscope is painful and the endoscopy is incomplete.

Our study aimed to design new surgical endoscope that can fulfill four important capabilities to tackle the problems mentioned: **bendability, trackability, stiffness adjustability,** and **controllability**. To attain the research aim, the idea is to design octopus-like soft robots actuated by pneumatic chambers. We improved previous pneumatic soft surgical robots (STIFF-FLOP) by increasing the number of chambers to four and merging stiffening and bending capability in each chamber. Benefits of having four chambers includes more intuitive control, antagonistic activation, and increase in resultant moment arm when activating two adjacent chambers. The embedding of stiffening sac into the chambers enable multi-level stiffness adjustment.

Mechanical experimentation is conducted to verify the intended mechanical capabilities. Our design (MOLLUSC) manipulator can bend up to 90°. With the inclusion of jamming material, four level stiffness is attained, however the bending performance is reduced. The four chamber designs improved two chambers bending angle compared to STIFF-FLOP. By freeing the robot from electromechanical components, it is possible to operate the robot under MR-scanner. The robot position can now be tracked using MRI. For the control, 2D control algorithm termed Passive Chamber Compensation (PCC) has been implemented with error less than 5°. For 3D control, the implemented algorithm is effective to achieve rotation angle multiple of 45°. Dynamic control is also verified. However, the robot traced rhombus shape instead of intended circular trajectory.

Acknowledgement

My biggest gratitude for God who has granted me courage, strength, and patience for this milestone in my life. Sincere thanks to my Prophet who introduced me to God and the beautiful way of life.

I thank my parent, my brother, and my wife for endless support until I can be where I am now.

I would like to thank *Lembaga Pengelola Dana Pendidikan (LPDP)* from Indonesian Ministry of Finance for supporting me with full scholarship. My study would not have been possible without their generous support.

My thanks also go to my supervisor, Momen Abayazid and Hamid Naghibi, for their support and guidance (and patience) that would make me possible to finish my master thesis.

Thanks for Lorenzo Masia and Prof Kees Slump for becoming my committee member.

Credit also goes to Jolanda for her support with all formalities, and the four technicians: Gerben, Sanders, Henni, and Marcel who has helped me greatly in the lab.

Thanks to Willem for the fruitful discussion about soft endoscope. Also, to Jorn who has developed the first control algorithm, and enable me to study greatly from his report. Thanks to Vincent for introducing me to the pneumatic components.

Thanks to my close friends in Enschede: Anas, Giri, Wasef, Mahmud, Bima, Asem, Abrar, and Dadi for the joyous time and pleasant stay in this rainy city. Thanks also for Mbak Nden and Mbak Ratna for the tasty (and sometimes free) food.

Table of Contents

List of Figures

List of Tables

1. Introduction

1.1. Context

With the recent trend in surgical operation field, surgeons have begun to move from open surgery to less-invasive and very recently non-invasive surgery. Open surgery is the very first established method of operation by incising the skin part outside of the organ to be intervened. Minimally invasive surgery is performed by introducing minimal incision in the nearest access point in patient body, and then place trocar that enables the instrument to get into the target organ (Figure 1.1). In this paradigm, surgeons operate the instruments from outside the patient body, unlike the open surgery in which the surgeons' hand directly control the device inside the surgery opening. Non-invasive surgery makes use of body natural orifice such as vagina or mouth for the surgical instruments to be inserted. In the minimally invasive and non-invasive surgery an endoscope that can be controlled remotely is used to access the organ (Figure 1.1).

The endoscope concept is that the proximal end of the device is controlled through the other distant end. This transmitted control enables the surgeons to control the device from outside the patient body. The transmission medium between the proximal and distal end of the endoscope can be either a rigid rod (coined rigid endoscope) or a flexible tube (termed flexible endoscope). At the distal end of the endoscope, surgeons can place camera and surgical instruments. Sometimes several endoscopes are used simultaneously to simulate surgeons' eye and two hands inside patient body.

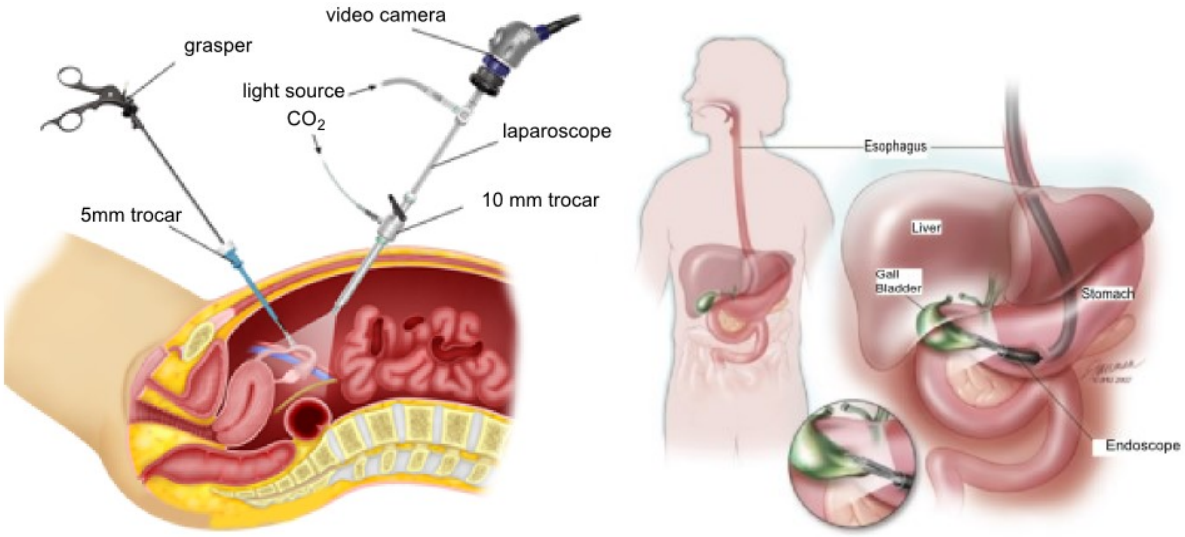

Figure 1.1 (left) rigid endoscope in operation[1]*), (right) flexible endoscope in operation*[2]

1.2. Limitation of Conventional Endoscope

The current endoscopic instruments pose several limitations for adaptation into minimally invasive and non-invasive surgery. As mentioned before, there are two types of endoscope: rigid and flexible endoscope. Rigid endoscope, while allowing stiff control of the endoscope, lessen the working space of the instrument because the rigid endoscope is passed through small trocar. This might pose a problem when the target organ is obscured by another organ or obstacle in line front of the target organ. The rigid endoscope mostly

cannot turn around to intervene the target organ [3]. Flexible endoscope, while allowing for better navigation inside the patient body, lacks the stability in doing the surgical intervention [4]. To make a precise incision, the stiffness of the distal end of the endoscope needs to be adjustable [5].

Another existing problem with endoscope is the localization of the endoscope inside the patient body [6]. In the usage of rigid endoscope, the localization is rather straightforward because the endoscope is not inserted deeply from the incision point. However, in using the flexible endoscope to trace a long lumen the view from the endoscope camera is not synchronized with how far the endoscope has gone inside the patient body. There is no way up to date to verify where the endoscope is inside the body. Moreover, the lack of depth perception and horizon stability make the localization of the endoscope even more challenging.

Another major limitation is the lack of controllability of the endoscope [7]. Rigid endoscope is clearly very limited in controllability. With flexible endoscope, while the distal tip can be controlled quite flexibly, the rest of endoscope tube cannot. To move the rest of the endoscope body, the surgeons need to push the endoscope. This method may result in the advancement of the distal tip to the wrong branch because of the lack of control combined with the lack of localization.

Other limitations that come from the pushing advance method of the endoscope are incomplete and painful endoscopy [8]. Incomplete endoscopy means the endoscope cannot reach the intended target. This may happen when the endoscope cannot advance in a sharp turn of the lumen. With current flexible endoscope, the lack of stiffness control might hinder the endoscope from moving forward and it will just form loop without being able to reach its target. On the other hand, there is a risk of damaging organ when rather stiff endoscope is pushed forcefully through the lumen. There is a need for variable stiffness segments of endoscope to be able to trace various turns inside of the lumen to avoid loop formation, while still enabling the flexible mode of endoscope to avoid painful pushing to the patient.

1.3. Research Question

To solve the endoscope design problems mentioned in the previous paragraphs, there are several key capabilities needed. First, for the endoscope to have flexible state and rigid state, the endoscope needs to have **stiffness adjustment** property. The endoscope also required to have **trackability** for the surgeons to localize the robot inside patient lumen. To tackle the maneuverability problem, the endoscope needs to have **bendability** and **controllability.** While bendability means the ability of the robot to bend, the controllability means the ability of the robot's segment to bend simultaneously in the predefined path/ angle calculated by a control system. Bendability and controllability, together with stiffness adjustment property are useful for preventing incomplete and painful endoscopy.

This study aims to develop the mechanical design, experimental characterization and control of single module soft surgical endoscope. We will focus on all four important aspects of surgical endoscope: stiffness adjustment, detectability, bendability, and controllability. This study will not cover the instrument dual arm design.

1.4. Thesis Outline

This thesis includes five chapters. After a general introduction to the endoscopes, the limitations in conventional endoscopes and the aim of the study in the current chapter (**Chapter I**), in **Chapter II** a more detailed literature review on soft robotics, including actuators, sensors, and control. Then the reader will be introduced to state-of-the art endoscope designs both from conventional and soft robotics. This chapter will

conclude with design concepts and specifications for future soft surgical endoscope. **Chapter III** will describe the design and fabrication technique to fulfill the design requirements. Chapter IV includes the mechanical characterization of the developed module. In **Chapter V** high-level control system based on constant curvature kinematics will be developed and validated both in 2D and 3D. Finally, in **Chapter VI** the improvements made by the developed endoscopic module, the limitation and suggestions for future research will be discussed, and the thesis will be ended with a conclusion.

2. Literature Review

2.1. Introduction

During a surgery, less incision will reduce patient trauma and recovery duration. Minimally Invasive Surgery (MIS) and Natural Orifice Transluminal Endoscopic Surgery (NOTES) are gradually replacing purely open surgery. One of the common applications of MIS or NOTES is endoscopy. The endoscope is originally a tool only to see the inside of patient lumen, but now it has developed into a tool for surgical intervention, especially with the increasing trend of MIS and NOTES.

The current interventional endoscopes are either rigid or flexible. The rigid endoscope is useful when the target organ is near incision point. Using rigid endoscope, the surgical operation can be performed with enough precision and force. When needed to reach distant organ, rigid endoscopes cannot circumvent a healthy organ. On the other hand, flexible endoscope is useful for reaching distant surgical target, and are already used in NOTES procedure such as colonoscopy. However, flexible endoscopes lack the stability required for distant surgical intervention [9]. Therefore, there is a need to introduce modern approaches to design the surgical endoscope.

Soft robotics, inspired by nature, is an emerging field in which flexible and compliant material is used to design and implement various robotic systems [10]. Soft robotics has several characteristics that may benefit its application in surgical robotics field. First, the robot bodies that is comprised from soft materials can comply with its surrounding environment, reducing potential of damaging tissue or organs. Second, the bendable characteristics of soft robots may provide the robotics endoscope the maneuverability to trace inside patient lumen [11]. Third, the soft robots may have the stiffness adjustable properties that enable the robotics endoscope the ability to stiffen intended part of its body [12]. Lastly, most of the soft materials used in soft robotics can be used inside MRI bore [13]. This can introduce an MR-compatible feature for endoscopes which can solve the endoscope localization problem.

Several articles have reviewed the medical robotics for MIS applications (e.g. [14]–[18]) most of which are outdated. Moreover, a few studies reviewed the recent developments in soft robotics actuators and sensors [19], [20]. Despite all the progress in implementation of soft robotics in medical robotics application in the last decade, a review on different concepts of the designs specifically developed for endoscopic applications is missing but can give a useful overview of the current state of the field. It can also provide an insight into the advantages and disadvantages of each mechanism for future developments.

This chapter aims to review the previous soft actuated endoscope designs. Several related areas will be highlighted. In the subsequent section, we will have a brief look at how biology has inspired the development of soft robotics followed by some highlights on current soft robotics technology in actuation, sensing, and control. Several State-of-the-art conventional and soft robotics technology in surgical endoscopy are reviewed, including: Invendoscopy, Neoguide, Minimally Invasive Neurosurgical Intracranial Robot (MINIR), Meshworm, and developments in the European project titled “Stiffness Controllable Flexible and Learnable Manipulator for Surgical Operation” (STIFF-FLOP) [21]–[24]. To conclude, we will provide new concept and design specification for future soft endoscope, based on the challenge in endoscope instruments as mentioned in chapter 1, state-of-the-art surgical endoscope, and possibilities enabled by soft robotics technology.

2.2. Method of Review

The key articles from soft robotics explain the knowledge of the field with specific highlight on the actuation, sensing, control, and stiffness adjustability of soft robots. A survey was performed to find the relevant articles on soft robotics Endoscopes, using *"Soft Robotics for MIS and NOTES" and "Soft Robotics Endoscope"* as keywords. The relevant articles on soft robot design that have been preliminary tested for surgical endoscopic applications were selected. Subsequently, three most pioneering soft robot designs were reviewed as: MINIR, Meshworm, and STIFF-FLOP. As comparison, conventional robotics solution for surgical endoscope, Invendoscopy and Neoguide, were also included. Moreover, the key cited articles in the references of these studies were also investigated.

2.3. Soft Robotics: Nature Meets Engineering

To gain insight into the soft robotics technologies, the current actuation and sensing technology used in soft robotics will be reviewed. The review will be followed by brief look at the stiffening mechanism of soft robots. The challenge for the control of soft robots will be shortly examined.

2.3.1. Actuators

This subsection will describe briefly some of the most common actuators used in soft robots [25].

Shape Memory Alloy: Shape Memory Alloy: The basic technology behind SMA is Nickel Titanium (NiTi) alloy wire that contracts under joule heating. Under cooling, the SMA reforms back to its initial shape [26]. The SMA wire can be used as agonist actuator to generate pulling force.

Cable actuators: The cable actuator derives its inspiration from tendon in human body. A motor is used to generate pulling force to the cables, which in turn move or pull rigid connecting plates between body segments to apply bending. Such approach is commonly used to control continuum robots.

Pneumatic Artificial Muscle (PAM): also known as McKibben actuator, this type of actuator is composed of inflatable elastic tube surrounded by a braided mesh. actuator contraction, elongation, and even stiffening can be achieved by changing the weave pattern and angle of the braided mesh. Typically, this kind of actuators works with driving pressure in the range of 0.34-0.68 MPa [27].

Fluidic Elastomer Actuator (FEA): a type of actuator that consist of soft elastomer layers separated by a flexible, but relatively inextensible constraint. The fluid pressure needed to actuate FEA is in the range of 0.02- 0.06 MPa. Many motion primitives are possible with FEA, including: extending, contracting, twisting, and bending. There is a variation of FEA in which fibers are used to reinforce the actuator. With the tradeoff of requiring higher pressure to activate (0.17- 0.24 MPa) the fiber reinforced FEA's can exert larger force, which may be needed for several applications [28].

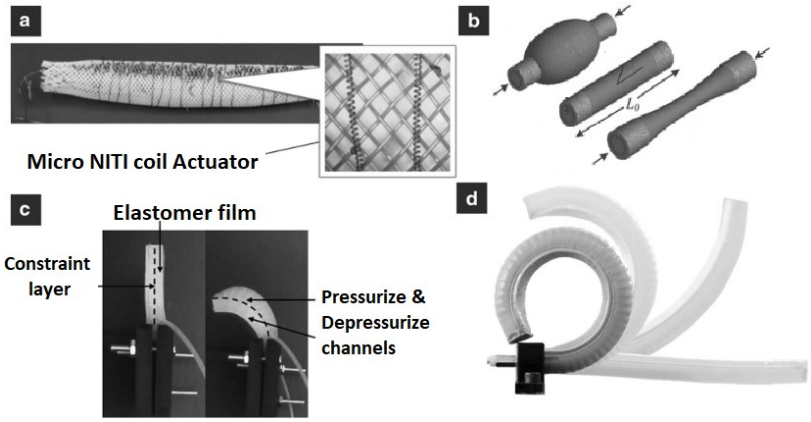

Figure 2.1 Common actuator for soft robots: (a) SMA actuator, (b) McKibben actuator, (c) FEA actuator, (d) Fiber-reinforced FEA [25]

Sensing is required for feedback control of the actuators. Three main requirements for integration of soft sensors are stated in literature [13]. First, the sensor must be compliant, so it does not affect the shape or the properties of the soft robot. Second, the sensor must be durable enough to stretch for many cycles of motion. Third, the sensor should not damage soft parts of the robot. There are several types of soft sensing currently employed in soft robotics design.

Resistive and Capacitive Stretchable Sensing: The largest challenge of soft sensors is the lack of elastic material with low elastic modulus that remain conductive at high strain [13]. Alternative approaches are passive resistive and capacitive element manufactured by embedding additives resistive or capacitive element into the elastomer matrix (example see Figure 2.2 left). However, the additive may stiffen the elastomer, so there is a trade-off between conductivity and softness of the robot.

Magnetic Sensing: Miniature magnet that exhibits Hall Effect is embedded in robot elastomer matrix to sense the strain of the robot (Figure 2.2 right). Non-contact nature of magnetic measurement has benefits including small dynamic artifacts, less effect on the mechanical properties of the elastomer, and small hysteresis [29].

Optoelectronic Sensing: another recent solution is to fabricate and integrate waveguides into the body of the soft robots. The power loss of the signal increases with increasing strain, because of longer pathways travelled by the light. The amount of signal loss can be used to deduce the shape of the robot [30].

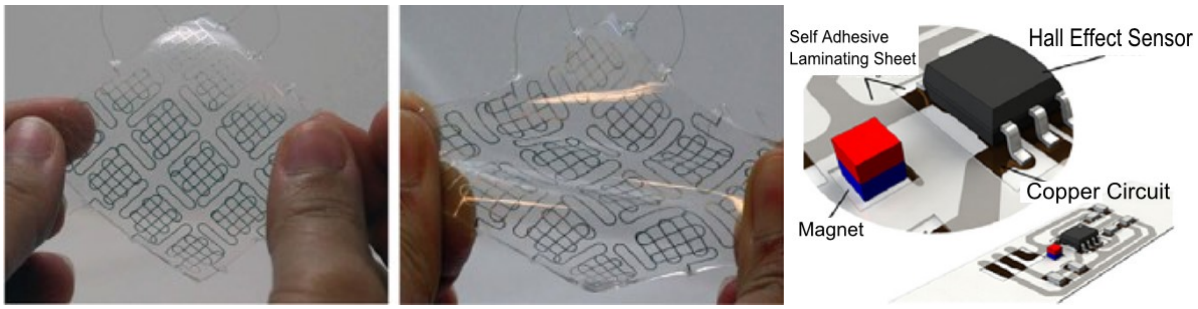

Figure 2.2 (left) stretchable conductors to measure strain via measured current, (right) magnetic curvature sensor comprised of a miniature magnet and Hall effect sensor, embedded on a flexible circuit [13]

2.3.2. Stiffening in Soft Robots

Currently, there are two ways of adjusting the stiffness in soft robots: using active actuators that are arranged in antagonistic manner and using semi active actuators that can change their elastic properties.

The antagonistic method exploits the use of active actuators that produce opposite force/ torque direction to each other (active-active) or are coupled with passive structure (active-passive) [12]. In nature, muscle co-contraction is an example of active-active stiffness adjustment, while muscle contraction and spring-like tendon is an example of active-passive stiffness adjustment. In soft robotics, the active-active pairs can be achieved by pairing any of the soft actuator mentioned in section 2.3.1.

Semi-active actuators work by modulating passive mechanical properties of the material itself. Examples include stiffness controllable material such as granular jammed membrane which stiffness can vary when vacuum is applied. Another example is electrorheological material (ERM) and magnetorheological material (MRM) that changes their stiffness when subjected to an external electric or magnetic field.

2.3.3. Control

Accurate position and motion control of soft robots remain an unsolved problem due to several high-level challenges. Soft sensors and actuators usually have non-linear dynamics, making model-based approaches difficult. Most soft materials have viscoelastic properties, which introduce hysteresis and subsequently large inaccuracies in open-loop control. Furthermore, integrated sensors are rare, complicating state estimation and feedback-control methods. Dynamics gets additionally complicated as fluidic soft actuators often exhibit slow response to pressure stimulus because of the delay caused by the time the fluid takes to fully enter the activated chamber [13].

2.4. State-of-the-art Robotics Endoscopes

Attempts have been made to design endoscopes that provide the four needed capabilities as mentioned in Chapter 1. Among the design from state of the art conventional robotics are Invendoscopy (Invendo Medical GmbH, Germany) and Neoguide (NeoGuide Endoscopy System Inc, Los Gatos, CA) [23]. These two robots are reviewed because they possess unique design ideas that might help in designing future endoscopes.

Invendoscopy consist of reusable single handheld controller, processing unit, and single use colonoscope [31]. The colonoscope can be inserted until as deep as 170 cm. The tip is bendable up to 180^0 in all direction (Figure 2.3). Tip bending radius of 35 mm enables retroflection and colon visualization. This endoscope also has a 3.1 mm working channel for housing surgical instruments. This robotic solution still uses manual insertion as its advancing method. Invendoscopy is already FDA approved.

Figure 2.3 (left) tip of Invendoscoy E200 [23]*, (right) NeoGuide* [23]

Neoguide colonoscope consist of 16 equally sized electro-mechanically actuated modules to form a snake like structure which can trace the lumen using computerized mapping [32] (Figure 2.3 right). The Neoguide uses programmable over-tube that prevents loop formation, thus avoid painful and incomplete endoscopy [33]. The tip of Neoguide can be guided to all direction [32]. The localization problem is tackled by external position sensor that measures the robot depth. Neoguide also enables two modes: passive and active. In the passive mode, the endoscope is relatively stiff. Multiple level stiffness control and independent stiffness control of each segment is not reported. The Neoguide is already approval by FDA.

2.5. State-of-the-art Soft Robotics Endoscopes

Adopting the beneficial properties of soft robots mentioned in section 2.3, soft robotics is slowly found its application in the design of surgical endoscopes. Among the research projects on this topic, we have Minimally Invasive Neurosurgical Intracranial Robot (MINIR), King's College London (KCL) Meshworm and Stiffness Controllable Flexible and Learnable Manipulator for Surgical Operation (STIFF-FLOP) [4], [21], [24]. Those soft robotics endoscopes will be discussed in term of four capabilities crucial for future endoscopes: stiffness adjustment, bendability, controllability, and detectability.

2.5.1. MINIR

MINIR robot is specially designed for endoscopy neurosurgery. The robotic design has three segments, with 60 mm total length and a diameter of 12.6 mm [21]. The robot has 3 mm diameter of free lumen that is used for electrocautery wires, and suction and irrigation tube. The robot has snake-like body composed of four disks interconnected by inner plastic springs. The outer part is covered by a long continuous outer spring. Each segment is activated by two pairs of tendons in an antagonistic manner which enable pitch and yaw motion. The tendons are actuated using SMA spring actuators. The robot material ensures its MR-compatibility [21].

MINIR uses central tendon routing mechanisms to actuate its body. In most of the existing robots with tendon driven mechanism, the cable routing is done in the peripheral part of the robot (see Figure 2.4 left, 1st configuration). This makes the movement of each segment coupled, as bending the distal end will give torque along all the robot body. In MINIR design, the cable branches out from central part of the robot toward the actuated disk (see Figure 2.4 left, 2nd configuration). In this fashion, if distal tip is activated, the proximal disk will only have compression force and not torque (see Figure 2.4 right).

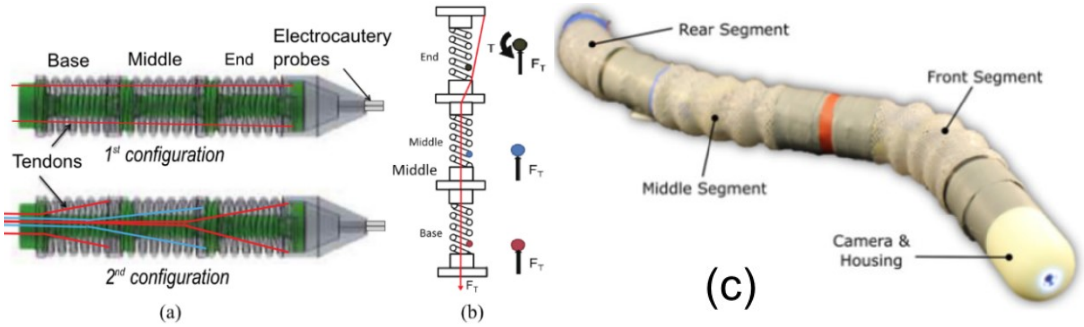

Figure 2.4 (a) Two configurations of tendon routing in continuum robot , (b) schematic of the forces acting in base disk when distal disk is bent according to cable routing of the 2nd configuration [21]*, (c) Meshworm robot* [24]

2.5.2. Meshworm

The Meshworm design, inspired by earth worm, is developed for colonoscopy application [24] (Figure 2.4c). This 50 cm lenght robot is composed of three segments made of soft plastic-silicone mesh composite. The outer diameter of the mesh is 31 mm when uncompressed and 35 mm when compressed [24]. Front and rear segments can bend about two axes, compress, and elongate. Each segment is actuated by tendon wound around pulleys which are mounted on DC motors. Locomotion is achieved by continuous anchoring, contracting, and un-anchoring of segments, like how earthworm crawls on the ground. Closed loop control is enabled by embedding Hall Effect sensor to indirectly calculate the length of each tendon. PID controller then will adjust the length of each tendon. The robot has free lumen, and in the prototype presented, an USB camera is mounted at the end tip.

2.5.3. STIFF-FLOP

STIFF FLOP is a surgical manipulator inspired by octopus arm [34]. As mentioned in [4], the STIFF-FLOP has evolved in three designs. In the first design of STIFF-FLOP, pneumatic actuation is employed to achieve multi-directional bending and elongation, while granular jamming is applied to vary the stiffness. The manipulator bodies are constructed from flexible and soft silicone elastomer, which enable the squeezing of the robot [34]. The robot consists of three fluidic chambers equally spaced in radial arrangement embedded in an elastomeric cylinder. The cylinder is then enveloped by a crimped sheath to limit the radial expansion of the chamber when inflated. Outer diameter of the overall module is 32 mm [34]. The granular jamming chamber is made of latex membrane filled with coffee powder and inserted in an 8 mm channel in the center of the STIFF-FLOP module. Jamming is induced by applying vacuum to the chamber. The design pursued by STIFF-FLOP used modular approach. Each module has the same stiffening and bending capability, and the length required for specific surgical purpose will determine how many modules are needed.

The first design of the STIFF-FLOP has several flaws which are addressed in the second design. One of the drawbacks is the reduction in chamber cross-section center when the chamber is pressurized. This cross-section center movement causes less bending moment. Another problem is the external sheath caused a friction between the sheath and the internal silicone, causing some actuation energy to be wasted in friction [35]. Fras et al. (2015) suggested three improvements: 1) removing the external sheath, 2) employ braiding on each actuation chamber, and 3) make the chamber into cylindrical cross-section [35]. The braided

chamber and cylindrical cross-section will allow more optimal elongation and limit the radial inflation[35]. Removal of external sheath eliminates the friction with internal silicone elastomer [35].

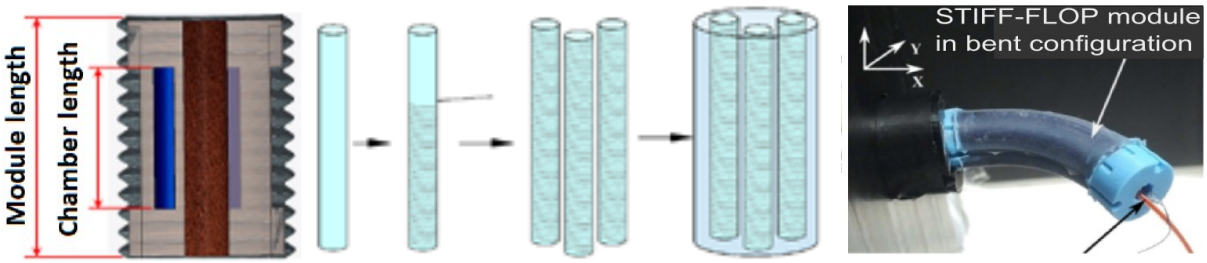

Figure 2.5 (left) The first design of STIFF-FLOP manipulator, with semi cylindrical pneumatic chambers and external braided sheath [36] *(middle) Improvements in the second design by using braided cylindrical pneumatic chambers [29], (right) 3rd design of STIFF-FLOP manipulator* [3]

The third design improves the second one by focusing on size reduction by excluding the central granular jamming membrane. The removal of this membrane opens space for free lumen inside the manipulator. Other improvement is the shift from one pneumatic chamber into a pair of pneumatic chambers. A pair of pneumatic chamber will make the resultant moment arm farther than single chamber, thus increasing the bending moment and stability [3]. Overall diameter of this third-generation design is 14.5 mm which fits into trocar for MIS operation. The two-module design had been implemented and tested in human cadaver and proved the reaching and bending ability of the manipulator [3].

2.6. Design Summary and Gap

Summary of the designs reviewed against the four crucial capabilities in designing endoscope can be seen in table 1.

Stiffness adjustment in the Neoguide and STIFF-FLOP robot are achieved by semi-active actuators (refer to section 2.3.C). In STIFF-FLOP, the granular jamming membrane is used. However, in the 1st design of STIFF-FLOP, the granular jamming membrane uses the central channel space which should have been used to house surgical instruments. The central lumen is emptied in the 3rd design of STIFF-FLOP at the cost of removing the central granular jamming mechanism.

All presented solution already fulfilled the bendability requirements. Tendon mechanism is used by all the presented solution except the STIFF-FLOP, which uses pneumatic actuation to bend its body. By trying to eliminate electric or magnetic field using soft robotics actuation, the integration of imaging modalities such as MRI scanner can solve the detectability problem. This approach has been used by MINIR to localize the robot [21]. Another solution for localization can be using depth position sensor like in Neoguide [23]. However, the use of EM sensor might interfere with MR imaging.

Table 2.1 Design Versus Specification for conventional and soft robotics endoscope solution

Design Specification	MINIR	KCL Meshworm	STIFF-FLOP 1st gen	STIFF-FLOP 3rd gen	Invendos-copy	Neoguide
Stiffness adjustment	✗	✗	✓	✗	✗	✓
Bendability	✓	✓	✓	✓	✓	✓
Trackability	✓	✗	✗	✗	✗	✓
Controllability	✓	✓	✓	✓	✗	✓

2.7. Future Endoscope Design Concept & Specification

After reviewing the state-of-the-art design, we would like to propose new concept for doing the endoscopic operation, which is by doing remote endoscopic operation under MR guidance [21],[37]. To tackle the endoscope localization problem, the endoscope will be placed inside an MR bore. The use of soft robotics will enable robot that is made from fully MR-compliant material, and by using pneumatic actuation, the pneumatic pipe can be elongated so the patient can be fully inside the MR-bore, while surgeons control the device in the vicinity.

The future development of soft robots in endoscopic application should covers the mechanical design of the robot. From controllability standpoint, bendable modular continuum robot already has both forward and inverse kinematic model [38], [39]. Because using sensing modality will interfere with the MR-compatibility of the robot, for our new surgical concept, open-loop control using kinematic model is preferable. The open loop control using constant curvature model has been tested in [3]. Instead of pushing the endoscope to make its way inside the lumen toward target organ, now it is possible to bend some segments of the robot to avoid painful endoscopy. The most advanced control possible using the kinematic model of modular continuum robot is the path planning algorithm toward the target like the one implemented in Neoguide [32].

Another consideration in endoscope design is the stiffness adjustability of the robot. It is preferable that the robot has several stiffness levels. This will be useful for different purpose, for example the most distal tip will be very stiff for making the surgical incision, the module before the most distal tip will become slightly less stiff to support the distal tip, while some other module far at the back will be stiff to support the bending of the robot while tracing the curve inside the lumen.

The modular design in all soft surgical robots reviewed is a promising approach in building continuum robots. The modular design facilitates the manufacturing process in blocks. Other benefit includes the flexibility to adjust the length of the robot as necessary for specific application. From the design point of view, first one module proof-of-concept design should be realized and tested, before moving to multi-module design.

Based on the new surgical concept we proposed, and considering the mechanical aspects of the design, the future soft surgical endoscope for NOTES application should fulfil the following specifications:

- Safe especially from pressure leakage
- Fully biocompatible and MR compatible material
- Bending in at least two antagonistic direction
- Bending angle of at least 90^0 for having lateral view

- Modularity
- Adjustable stiffness in at least two levels
- Internal free central channel to house surgical tools such as endoscopic camera
- Able to deliver force between 0.9 and 3.3 N [14

3. Mechanical Design of Multi-Level Stiffness Controllable (MOLLUSC) Endoscopic Module

3.1. Design platform: STIFF-FLOP[1]

This design is based on the STIFF-FLOP manipulator introduced in previous chapter. The STIFF-FLOP uses three radially arranged expandable chambers to achieve its bending and one granular jammed central channel to achieve its stiffening. The chambers are expanded pneumatically. Design of 1st generation STIFF-FLOP module can be seen in Figure 3.1. Under the activation of one bending chamber, the actuator will bend to the opposite direction (Figure 3.1). Under the activation of two chambers, the actuator will bend to the direction opposite to the central line between the two activated chambers. Actuating the three chambers together will elongate the manipulator. Experimental characterization of the STIFF-FLOP design is presented in Table 3.1.

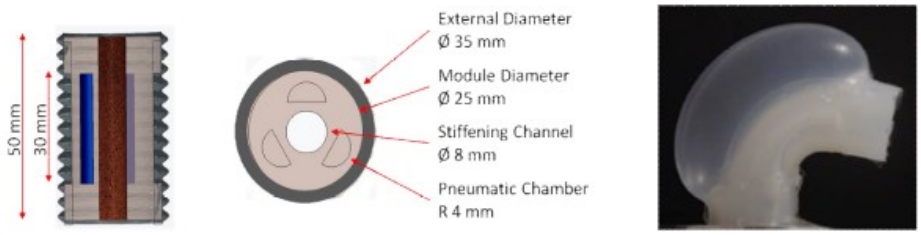

Figure 3.1 (left)The structure of STIFF-FLOP actuator, (right) bending of the STIFF-FLOP actuator without the external braided sheath [36]

Table 3.1 Mechanical Design Characteristic of STIFF-FLOP 1st generation module [36]

Characteristic	Pressure condition	Value
Maximum one chamber bending angle	0.65 bar	120°
Maximum two chambers bending angle	0.65 bar	80°
Maximum elongation	0.65 bar	86.3%
Maximum force at one chamber bending	0.65 bar	24.6 N
Maximum force at elongation	0.65 bar	41.4 N
Maximum stiffness variation	Base condition (no pressure)	36%

One counter-intuitive characteristic is that pressurizing two chambers simultaneously reduces the bending angle than pressurizing one chamber. The reduction at 0.65 bar can reach value of 40° (Table 3.1). In STIFF-FLOP design, all chambers are separated by 120^0. Denoting cross-section of one chamber as *r*, activating two chambers together should make the resultant moment arm to be *r.* Therefore, activating two chambers simultaneously ideally should keep the same resulting bending angle. Moreover, analysis from STIFF-FLOP design mentioned chamber cross-section center displacement toward the center of the module, causes further reducing the resultant moment arm [35]. This resulted in less bending from two chambers bending in STIFF-FLOP [36] .

[1] This is the second design that we tried. The first design has issue with the tubular bending of the actuator. Detail of first design can be read in appendix A.

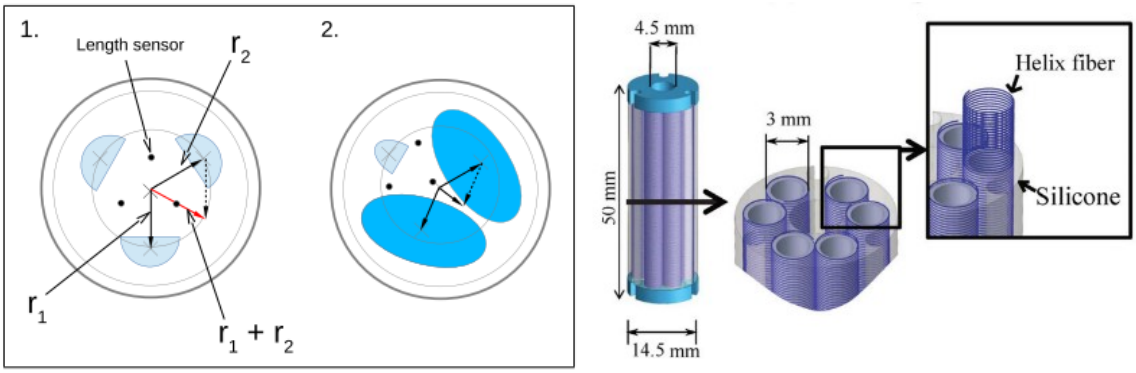

*Figure 3.2 (left) analysis of STIFF-FLOP design by Fras et al (2015), (1) depicted the non-actuated state, (2) depicted the actuated state. The resultant bending angle of simultaneous chamber activation is less than r1+r2 [*35], (right) *module design of third generation of STIFF-FLOP manipulator* [3]

In the third-generation design of STIFF-FLOP, the development was more focused toward MIS application and the target was to decrease the size of the module. Moreover, with the specific aim to use the STIFF-FLOP with a camera, the stiffening chamber was no longer implemented (Figure 3.2). There is positive aspect of the third design such as more efficient bending using a connected paired chamber. However, with the elimination of stiffening mechanism, the design is no longer fulfilling the need for stiffness controllable surgical tools for MIS and NOTES application.

3.2. Improvements of STIFF-FLOP design

As discussed previously, STIFF-FLOP has stiffness adjustment ability with the drawback of not having the free central lumen. The third design has central free lumen with the drawback of eliminating the stiffness adjustment ability. In the current study, we build a new design based on STIFF-FLOP concept to achieve both free central lumen and stiffening as well as bending capabilities.

The first novel design concept that we propose in this work is the combination of granular jamming and actuation in one chamber. This combination of function will optimize the space inside the module. In our design, we achieve this by inserting the granular jamming sac inside the actuation chamber. By using solenoid valve, we can switch the input to the chamber either by vacuum line (for granular jamming) or by pressure line (actuation).

The second improvements made by our concept is that multi-level stiffening can be gained. First, we achieve this by controlling the vacuum level of the chamber. The second way of controlling the stiffness can be by activating one or several chambers. As the stiffening component was moved from central chamber to the side chambers, now different combination of chambers can be used which enables multi-level of stiffening: one chamber, two chambers, three chambers, and four chambers stiffening.

Other modification is the increase of number of chambers from three to four. Four chambers will make the control more intuitive because it will correspond to front, back, left, and right. By activating two adjacent chambers, four more secondary directions could be achieved, resulting in total bending of eight directions. Furthermore, with four chambers the number of stiffening levels can be increased even further (four chambers stiffening). Besides, using four chambers, arranged in two paired chambers, enables antagonistic actuation. By using antagonistic actuation, it is possible to modulate the actuator stiffness in specific pose

(like muscle co-contraction). This modulation will enable more precise force exertion and better control [40].

Four chambers design hypothetically exhibit an increase in the moment arm in case of two chambers activation (Figure 3.3). In the case of three chambers design, the angular distance between chambers is 120°. Simultaneous activation of two adjacent chambers will result in moment arm of r. In case of four chambers design, the angular distance between chambers is 90^0. Therefore, activating two adjacent chambers will result in moment arm of $r\sqrt{2}$. Although the chamber cross-section center of our design will also displaced toward the center [35], we expect resultant moment arm to be longer than STIFF-FLOP.

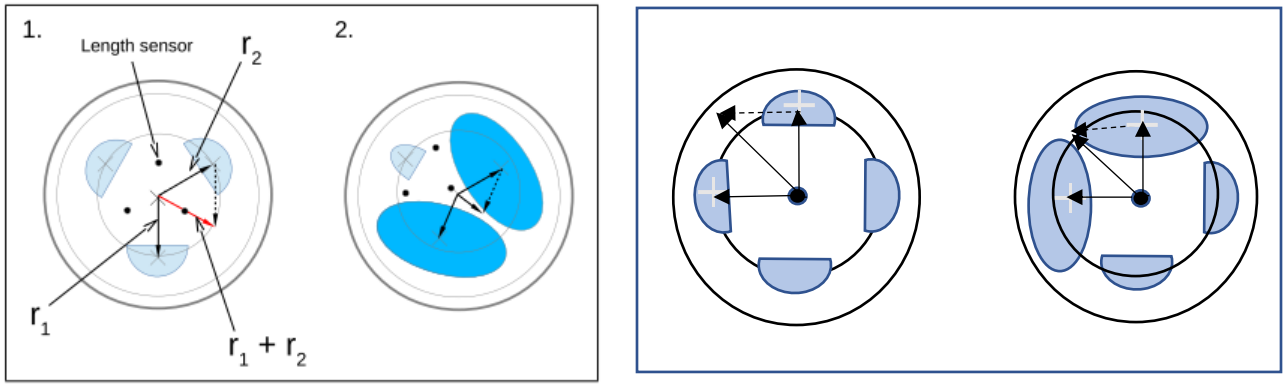

Figure 3.3 (left) cross-section center displacement in STIFF FLOP design, 1 depicts unactuated state, 2 depicts the actuated state, the resultant vector of two actuated chambers cross-section center is decreased [35], *(right) the resultant cross-section center in our design is also decreased, but not as much as in* [35] *because the angle between chambers is 90^0 instead of 120^0 so the net resultant vector is $r\sqrt{2}$ instead of r*

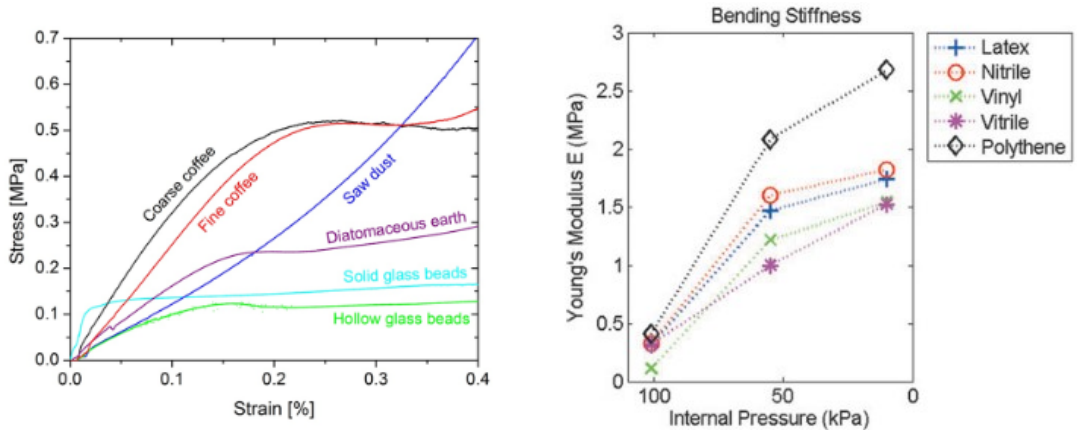

Figure 3.4 (left) compressive stress versus strain verified that coffee is the most suitable material for granular jamming grains [41], (right) bending stiffness comparison of several granular jamming membrane under vacuum pressure [42]

For the granular jamming material we used coffee powder. Analysis from Cheng et al (2012) verified that ground coffee has high strength-to-weight ratio in addition to large absolute strength [41] (see Figure 3.4). Therefore, ground coffee is the chosen material in our application.

The last modification is the jamming membrane. For the material of granular jamming sac, latex rubber and neoprene were compared. Qualitatively, latex resulted in lower stiffness than neoprene when vaccuumed. In previous research, it is found that latex is not the most ideal granular jamming membrane, and the polythene rubber outperforms latex for vacuum stiffness in bending, tension, and compression testing [42] (Figure 3.4). Considering the above finding, unlikr STIFF-FLOP we used neoprene for capsulatinf the jamming material.

3.3. Design Overview

In short, first novelty of our design with respect to STIFF-FLOP is freeing the central lumen by moving the stiffening mechanism to every chamber. The chamber now can be used for both bending and stiffening. In addition, vacuuming the chamber individually will enable multi stiffness level. Other novelty is arranging the chambers in two antagonistic pairs, which will allow more intuitive control of bending and an increase in resultant bending angle. The use case scenario of our manipulator, which exploits multi-level stiffness capabilities, can be seen in Table 3.2 – Table 3.6. Drawing of the design can be referred to Figure 3.5.

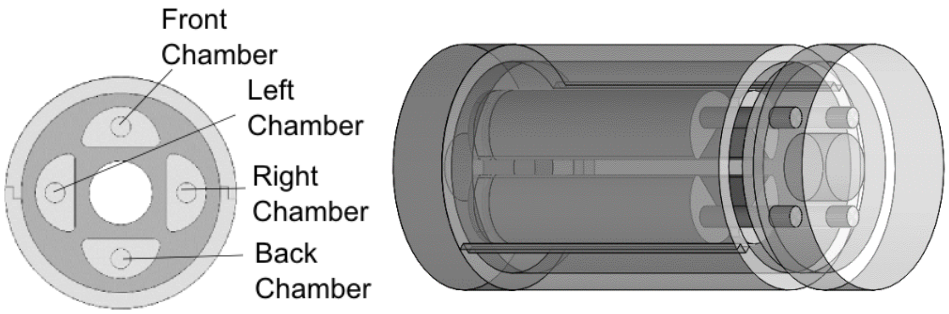

Figure 3.5 design of the proposed MOLLUSC (Multi LeveL Stiffness Controllable) manipulator (left) top view of the mold, (right) side view of the mold

In the following, the new design is named MOLLUSC (Multi-LeveL Stiffness Controllable) robot. The biological inspiration of stiffness adjustable manipulator comes from octopus, and octopus fall under the taxonomy of mollusk. Hence, we give the name MOLLUSC aiming that the robot will mimic the ability of octopus arm.

Table 3.2-Use case scenario for MOLLUSC manipulator in base condition (+ denotes positive pressure, - denotes negative pressure, 0 denotes neutral)

Use Case Number	Scenario	Chamber 1 (right)	Chamber 2 (front)	Chamber 3 (left)	Chamber 4 (back)
1	Base condition	0	0	0	0
1a	Base condition stiffness level 1	0	0	0	-
1b	Base condition stiffness level 2	0	-	0	-

Use Case Number	Scenario	Chamber 1 (right)	Chamber 2 (front)	Chamber 3 (left)	Chamber 4 (back)
1c	Base condition stiffness level 3	0	-	-	-
1d	Base condition stiffness level 4	-	-	-	-

Table 3.3-Use case scenario for MOLLUSC manipulator in one chamber bending condition (+ denotes positive pressure, - denotes negative pressure, 0 denotes neutral)

Use case Number	Scenario	Chamber 1 (right)	Chamber 2 (front)	Chamber 3 (left)	Chamber 4 (back)
2	Left bending	+	0	0	0
2a	Left bending Stiffness Level 1	+	0	-	0
2b	Left bending stiffness level 2	+	-	0	-
2c	Left bending stiffness level 3	+	-	-	-
2d	Left bending stiffness level 4 (release the air that causes left bending, and stiffen that chamber)	-	-	-	-

Table 3.4-Use case scenario for MOLLUSC manipulator in two chambers bending condition (+ denotes positive pressure, - denotes negative pressure, 0 denotes neutral)

Use case number	Scenario	Chamber 1 (right)	Chamber 2 (front)	Chamber 3 (left)	Chamber 4 (back)
3	Back left bending	+	+	0	0
3a	Back left bending and stiffening	+	+	-	-

Table 3.5-Use case scenario for MOLLUSC manipulator in elongation condition (+ denotes positive pressure, - denotes negative pressure, 0 denotes neutral)

Use Case Number	Scenario	Chamber 1 (right)	Chamber 2 (front)	Chamber 3 (left)	Chamber 4 (back)
4	Elongation level 1	+	0	+	0
4a	Elongation level 2	+	+	+	+
4b	Elongation and stiffening	+	-	+	-

Table 3.6-Use case scenario for MOLLUSC manipulator in three chambers bending condition (+ denotes positive pressure, - denotes negative pressure, 0 denotes neutral)

Use case number	Scenario	Chamber 1 (right)	Chamber 2 (front)	Chamber 3 (left)	Chamber 4 (back)
5	Left bending three chambers	+	+	0	+
5a	Left bending three chambers and stiffening	+	+	-	+

3.4. Fabrication

In this section the material and molds required for fabricating a single module robot will be discussed. Next, the manufacture of each part of the robots is described. Finally, the assembly and integration of the soft robot will be explained. The complete list of materials is listed in Appendix B.

3.4.1. Robot body fabrication

To Fabricate the robot body, first we printed the mold using 3D printer (Objet260 Connex3, StrataSys Inc), in Verowhite and Veroclear material (Vero material, StrataSys Inc). Vero material is chosen not to make the mold sticky after its curing. In the previous design (the antagonistic pneunet – see appendix A) a PLA mold was tried out, and the material sticks very hard to the mold, making the removal of the cured elastomer difficult. Moreover, spraying at the molds using release agent will make the removal process of cured material easier.

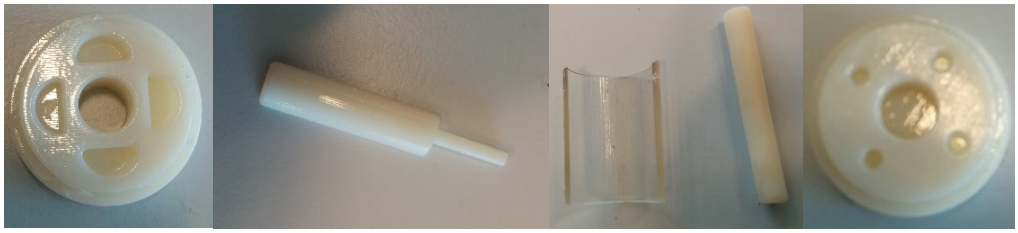

Figure 3.6 mold of MOLLUSC manipulator, from left to right: cap_A, chamber, shell and central cylinder, cap_B

To process the silicone elastomer, first part A and part B of Ecoflex silicone (Ecoflex, Smooth on Inc) were mixed with 1:1 weight ratio. After that, the mixed material is vacuumed (-0.9 bar) for about 5 minutes to remove the air bubbles. After making sure that there is no bubble, we proceed to slowly pour the material into the molds.

The molding process itself consist of two parts. First, the part that has the chamber is placed at the bottom, and the material is then poured until the edge of the shell (See Figure 3.7 a, b). After the first mold is cured, the module was reversed, and the chamber was inserted into cap B so the small part of the chamber is at the bottom. The shell was arranged until it was parallel to the central cylinder. The material was poured until the edge of the shell (see Figure 3.7 c-f). For the module without the granular jamming, after the silicone is cured, we inserted 2mm diameter silicone tube with silicone adhesive.

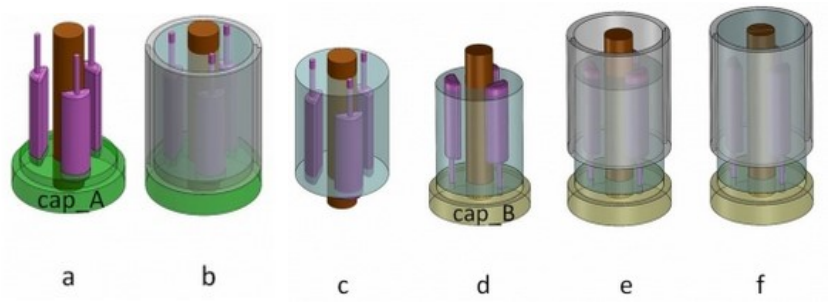

Figure 3.7 molding process of MOLLUSC manipulator, (a, b) the first part of molding, (c-f) the second part of molding [43]

3.4.2. The Braided Sheath & Granular Jamming Membrane

To arrange the robot sheath, braided sleeve with minimum diameter of 10 mm and maximum diameter of 25 mm (RS 408-249, RS Components) was inserted into a 30 mm dimeter cylinder. The sleeve was then pushed down until crimped structure was formed. The structure was heated with a heat gun until the crimps was hardened with care for not melting the sleeve.

For the granular jamming membrane, first we cut the neoprene from neoprene gloves one half section of the little finger. This glove is filled with one gram of coffee powder. For the tube, first we cut cone section of the tea bag filter and wrapped it around the tube using thread and parafilm. Finally, the capped tube was inserted into the granular jamming sac and further wrapped using parafilm. The complete granular jamming sac can be seen in Figure 3.8 c.

(a) *(b)* *(c)*

Figure 3.8 (a) the cable sleeve for robot sheath, (b) the crimps are formed around the cylinder and heated [44] *(c) a granular jamming sac*

3.4.3. Components assembly

To integrate all parts, the granular jamming sac needed to be inserted from the bottom part of silicone chamber. To do this, the sac fist needed to be stiffened by vacuum. The stiffened sacs were then pressed to have similar shape with the chambers. The sacs could then be inserted into the module. The ready braided sheath was donned from the upper part of the module. We could also put a silicone tube inside the central channel to simulate channel for cables/ surgical instrument. The complete robot can be seen in Figure 3.9.

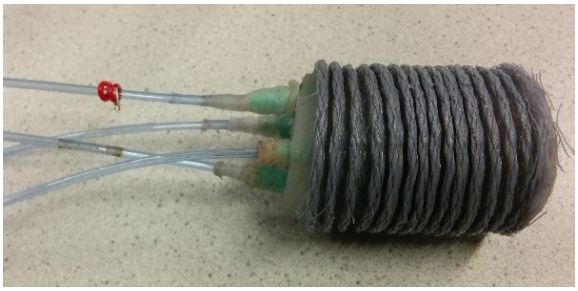

Figure 3.9 manufactured MOLLUSC manipulator

3.5. Low-Level Control System

A low-level control system for the MOLLUSC was developed as demonstrated schematically in Figure 3.10 to perform the charecterization experiment. Each chamber can be connected to a pressure line for actuation or vacuum line for stiffening using a switching valve. The pressure and vacuum can be adjusted using digital regulators. The pressure/ vacuum from digital regulator is first fetch into on/off solenoid valve. A switching solenoid valve in front of the two on/off valves will choose between delivering pressure/ vacuum to one chamber of actuator. In current implementation, for on/off valve, we used simple mechanical on/off valve, and for the switching valve, we used MHE series solenoid valve from Festo Inc. For the digital pressure regulator and vacuum regulator, we used positive and vacuum VEAB pressure regulator from Festo Inc respectively. With this configuration, working pressure from -1 to 1 bar is fetched to the actuator. This control system will ensure any of the chamber in either pressurized state, normal state, or vacuum state simultaneously to fetch all combination of state in the use case scenario mentioned in section 3.3.

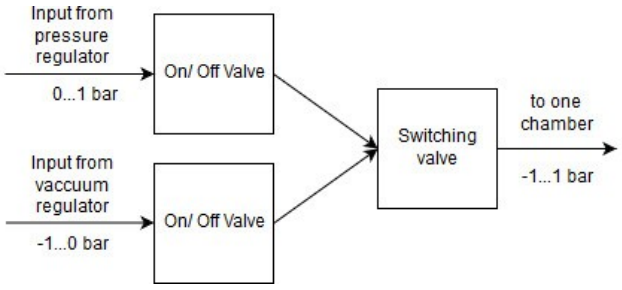

Figure 3.10 control system to actuate one chamber of MOLLUSC actuator

4. Experimental Characterization of MOLLUSC Endoscopic Module

After developing the MOLLUSC, the module needs to be characterized in terms of bending, elongation, stiffening, and the exerted force. We examined the effect of adding granular jamming to the bending and elongation of the robot. The other testing includes observing the force exerted by the module and the stiffening capabilities. Some of the results will be compared with the previously developed STIFF-FLOP.

4.1. Aim of the Experiments

In details, there are 6 characteristics that are observed: 1) maximum pressure, 2) pressure versus bending one chamber, 3) pressure versus bending two chambers, 4) pressure versus elongation, 5) pressure versus force, and 6) stiffness characteristics. Maximum pressure testing aims to determine the safe pressure that can be applied to the chamber to avoid chambers explosion. Pressure versus bending testing aims to answer the research question of achieving **bendable** soft endoscope. We will also examine the effect of pressurizing one chamber and two chambers simultaneously with the same amount of pressure. Pressure versus elongation will see how much the robot will elongate under simultaneous pressure. This elongation can add to the active robot degree-of-freedom and may enable more dexterous maneuvering of the robot. Force testing will check how much force the robot can apply and see whether it fulfills the specification mentioned in section 2.7. Finally, the stiffness testing aims to verify and quantify the **stiffness adjustability** of the robot in base condition and one chamber bending use case scenario (see Table 3.2 & Table 3.3).

4.2. Experiment Setups

This section will explain the setup for each of the testing mentioned above. In general, the pressure was supplied using manual regulator and read by digital manometer.

4.2.1. Maximum Pressure

The testing setup is as follow. One of the chambers was connected to the pressure regulator. Then, the pressure was increased in 0.05 bar step until either: 1) the chamber exploded, 2) the robot achieved 180° bending, or 3) the pressure regulator achieved its maximum pressure of 1 bar. By achieving a bending angle of 180°, the robot can already have almost fully spherical field of view, therefore there is no need to increase the bending (and pressure) any further. This test was conducted on the MOLLUSC version without and with the granular jamming material.

4.2.2. One chamber bending

Based on the result of maximum pressure testing, the pressure fetch to module without granular jamming was set up to 0.45 bar to prevent leakage. The pressure fetch to module with granular jamming was set to be until 0.7 bar to prevent chamber failure. Pressure was increased from 0 to the maximum pressure with step of 0.05 bar. The resulting bending angle is captured by camera and measured in imageJ software. This testing is performed on all four chambers. Each chambers data is taken in five repetitions.

4.2.3. Two chambers bending

In two chambers testing, the pressure is supplied to two adjacent chambers simultaneously. The range and step of supplied pressure is the same as one chamber bending testing. The resulting bending angle is captured by camera and measured in imageJ software. In taking the picture, the camera shot is perpendicular to the direction of bending. This test was conducted on all four possible combinations of adjacent chambers. Each chamber combination testing was repeated five times.

4.2.4. Pressure versus Elongation

For elongation testing, two opposite chambers and all chambers are pressurized simultaneously. The strain or elongation is defined as the length difference of the module at any given pressure with initial length at pressure of 0 bar, defined in the percentage of initial length. The test was done two times for module with granular jamming, and one time in module without the granular jamming. In the 2nd testing with granular jamming module, the bottom part of the chamber was slightly torn, therefore it was only possible to pressurize the module pressure up to 0.6 bar.

4.2.5. Pressure versus Force

For measuring the force, we performed vertical force testing. This experiment was performed by placing an ATI mini 45 load cell on top of the robot, and then pressurizing the robot up to 0.75 bar with step of 0.05 bar. The vertical movement of the robot is constrained by the sensor; therefore, the vertical force is exerted on the sensor. The vertical force testing is done for two chambers elongation and four chambers elongation.

4.2.6. Stiffening testing

For stiffening testing, ATI mini 45 load cell was mounted in a slider and the slider was held by laboratory clamp (Figure 4.7 inset). The slider was then placed just to touch the actuator from lateral slide. We then imposed displacement from 1 mm to 15 mm with a step of 1 mm, using the slider. The reaction force of MOLLUSC manipulator was recorded in each data point. We recorded the force in line to the direction of displacement. The stiffening experiments were performed for the robot in base condition and in one chamber bending condition with various stiffening level (use case scenario in Table 3.2 & Table 3.3). The pressure fetch to bend the manipulator was set to be 0.65 bar.

4.3. Results

4.3.1. Maximum Pressure

Results for module without granular jamming can be seen in Table 4.1. Applying pressure of 0.8 bar will result in almost 180° bending, therefore we stopped at 0.8 bar. Two of the chambers could not achieve 180° because of air leakage. The leakage also led to noisy screeching sound. It is observed that in front chamber the leakage happened between 0.5 and 0.55 bar, and in right chamber the leakage seemed to happen since very low pressure. In two chambers bending, the behavior of bending followed the most sensitive chamber.

Three of four possible chambers combination could achieve bending of almost 180°. The only exception was back right bending, which is comprised of two rather defect chambers, which resulted in less achievable bending angle.

Table 4.1- maximum pressure versus bending angle characteristic for module without granular jamming

Chamber	Maximum pressure (bar)	Reason of stopping at maximum pressure	Bending angle at maximum pressure (°)
Right	0.8	The chamber leaked very badly	129.5
Left	0.8	Almost 180° bending	177.3
Back	0.8	Almost 180° bending	173.2
Front	0.8	The chamber leaked very badly	128.3
Right + front	0.8	The chamber leaked very badly	111.5
Right + back	0.8	Almost 180° bending	166.2
Left + front	0.8	Almost 180° bending	168.9
Left + back	0.8	Almost 180° bending	171.8

For module with granular jamming, one chamber exploded at pressure above 0.8 bar (Table 4.2). The other chamber (left) could withstand pressure until 1 bar, which is the maximum pressure the pressure regulator can deliver (Table 4.2). Although left chamber did not explode, the granular jamming sac started to push the chamber through the bottom side. Examining the chamber failure (Figure 4.1), we observed that front chamber failed by explosion of coffee powder at the bottom part of the chamber. This pressure from granular jamming sac also tear the bottom part of the module (Figure 4.1).

Table 4.2- maximum pressure versuss bending angle characteristic for module with granular jamming

Chamber	**Maximum pressure**	**Reason of stopping at maximum pressure**	**Bending angle at maximum pressure (°)**
Front	0.8	The chamber exploded	67.4
Left	1	Maximum pressure of the regulator	112.1

Figure 4.1 (left) the failure at the bottom part of front chamber, (right) the bottom part of front chamber is torn

4.3.2. One Chamber Bending

The results of the bending experiment were presented in Figure 4.2. Each graph can be divided into three zones. One zone is zero bending angle, then the gradient started to appear with low value, and after some value of pressure the gradient suddenly rises.

First difference between the module with and without the jamming material can be seen in the starting point of module response to pressure. The starting point of module without jamming is 0.15, while with jamming material it became 0.3 bar. The second difference is the achievable bending angle. Without jamming material, with a pressure of only 0.45 bar, the module can bend to 90°, While with jamming material, with 0.7 bar pressure, the bending is only 50° in average.

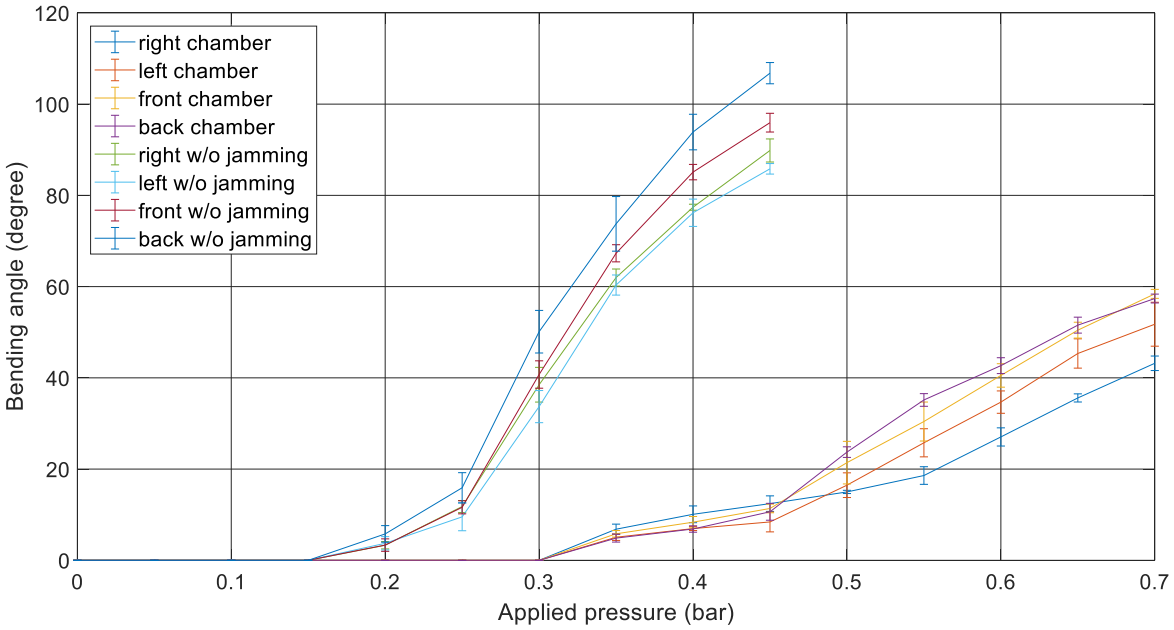

Figure 4.2 pressure versus bending angle characteristic for one chamber bending

4.3.3. Two Chambers Bending

The results of two chambers bending were illustrated in Figure 4.3. The graphs of two chambers bending also showed three zones of the curve: the flat zone, the zone with low gradient, and the zone with higher gradient. The starting point of the module response in two chambers bending is the same with one chamber bending. The difference of the two groups (with and without granular jamming) includes the achievable maximum bending angle. Two chambers bending in module without jamming material achieve an angle of 80°, while in module with jamming material the angle is about 50°.

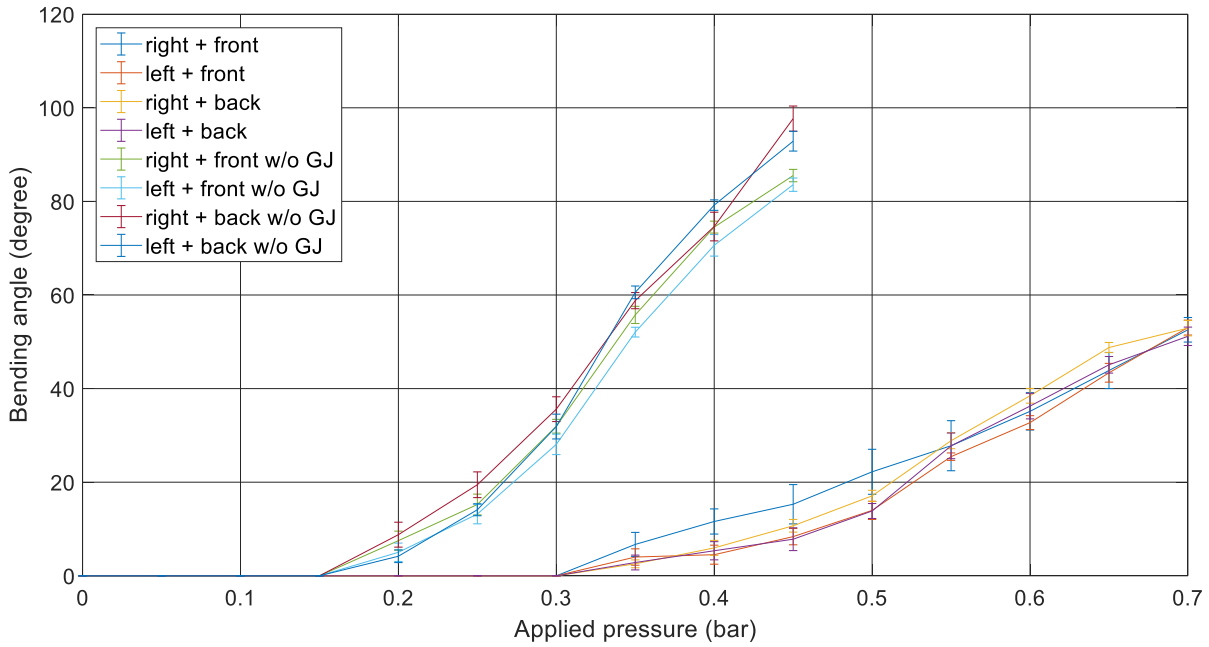

Figure 4.3 pressure versus bending angle characteristic for two chambers bending

Figure 4.4 summarizes the difference between the pressure versus bending effect on one and two chambers. With jamming material, the maximum achievable bending angle is less than without jamming material. Both bendings (one chamber and two chambers) showed similar behaviour with granular jamming material, whereas without jamming material, the one chamber bending showed slightly larger bending of about 10°.

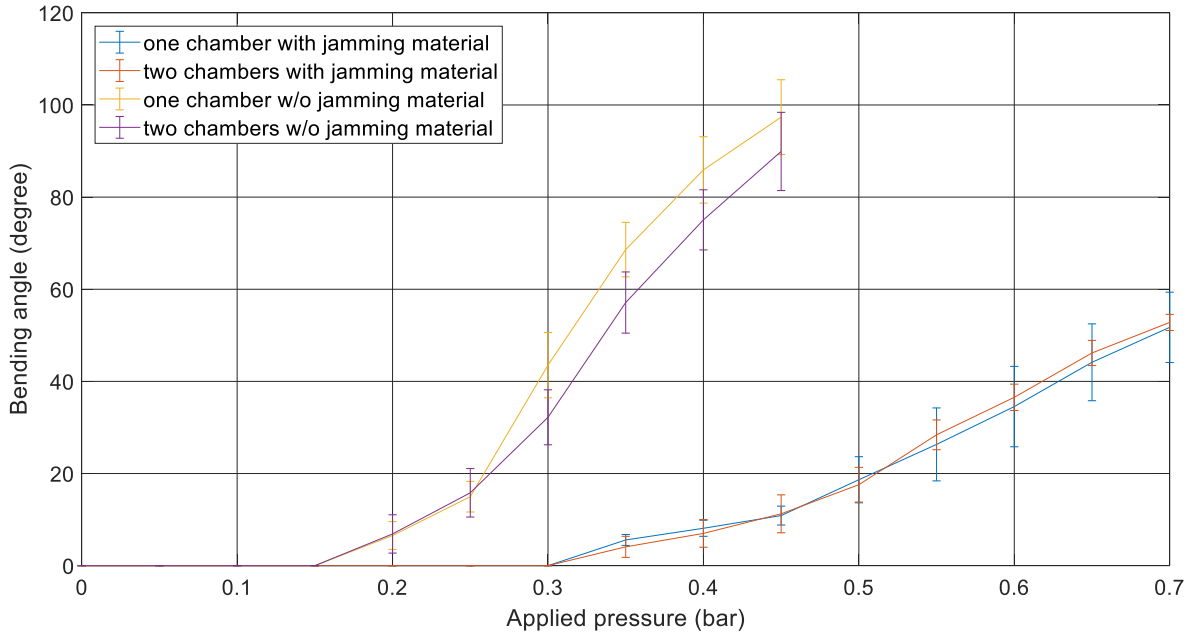

Figure 4.4 pressure versus bending angle characteristic for one and two chambers bending

4.3.4. Pressure versus Elongation

Figure 4.5 illustrates the results of the elongation experiments. In STIFF-FLOP first design, it is reported that maximum elongation achieved at 0.65 bar is 86.3% [36]. In our design, the maximum achievable elongation in module without jamming is 43%, around half of the STIFF-FLOP module. In the module with jamming, the highest elongation achieved is 70%.

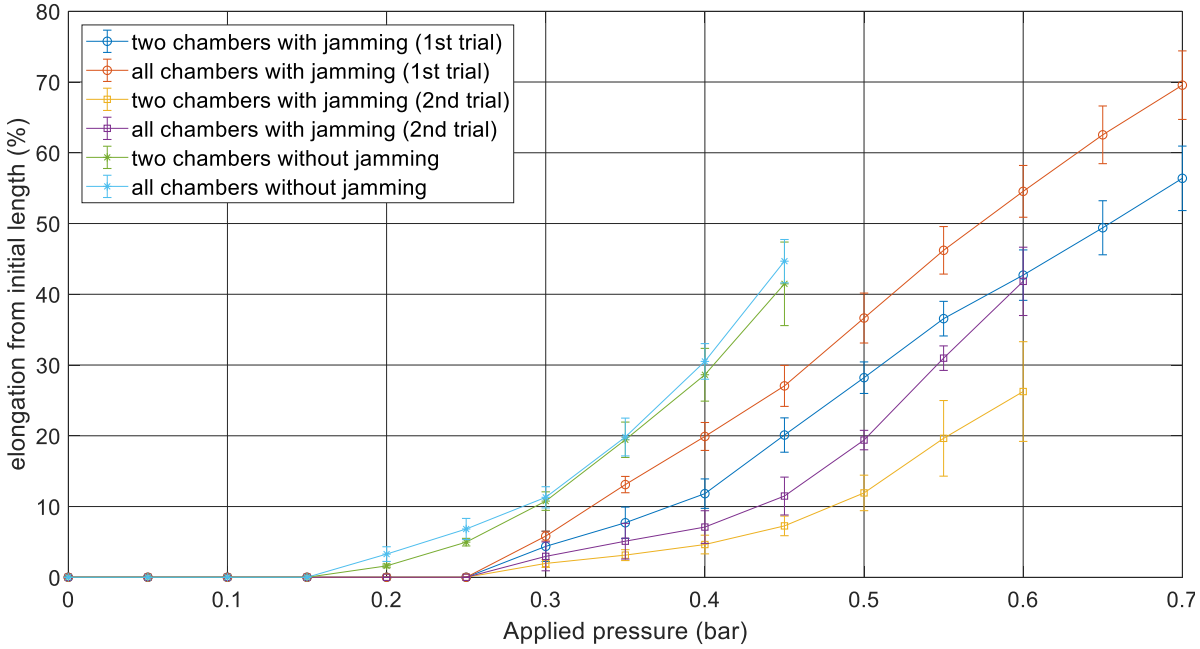

Figure 4.5 pressure versus elongation graph for module with and without jamming

4.3.5. Pressure versus Force

From Figure 4.6 pressurizing four chamber always give more force than pressurizing two chambers. The maximum force of the module at 0.75 bar with two chambers elongation is 11.47 N. With four chambers elongation, the maximum force increases to 18.88 N. This corresponds to an increase of 65% in the applied force (Table 4.3).

Table 4.3-force delivered at various numbers of activated chamber

Condition	maximum force @0.75 bar (N)	% increase from two elongation force
two chambers elongation	11.47	0
four chambers elongation	18.88	65

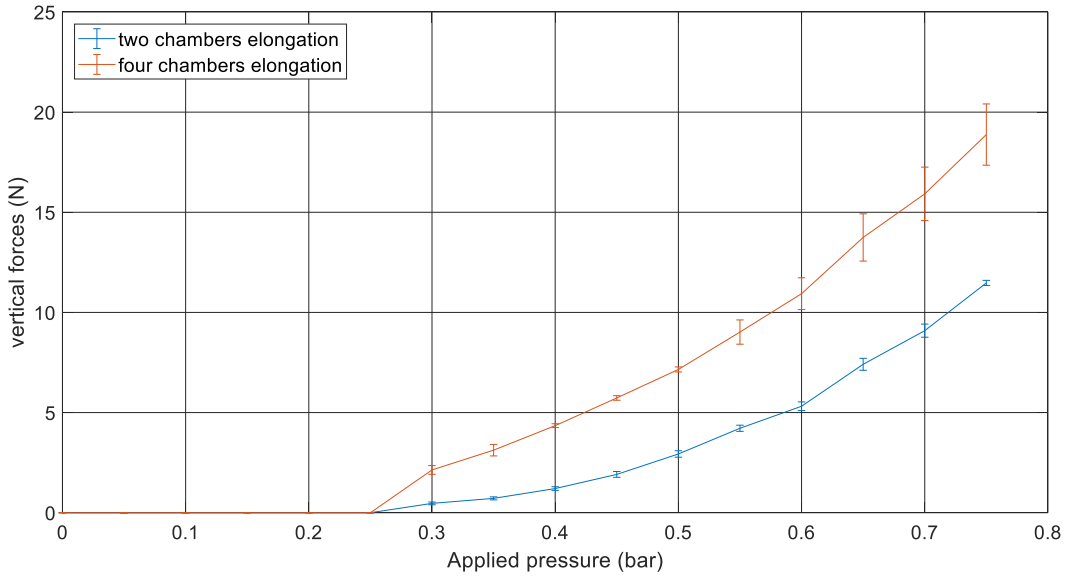

Figure 4.6 pressure versus force graph for module with jamming

4.3.6. Stiffening Testing

Results of stiffening testing in base condition can be seen in Figure 4.7. For level 2 stiffening, the stiffness increase was observed to be in the region of displacement after 10 mm. In level 2 stiffening, the two stiffened chambers were the chambers in the direction of applied force. For level 4 stiffening, the stiffening effect was observable in almost all displacement.

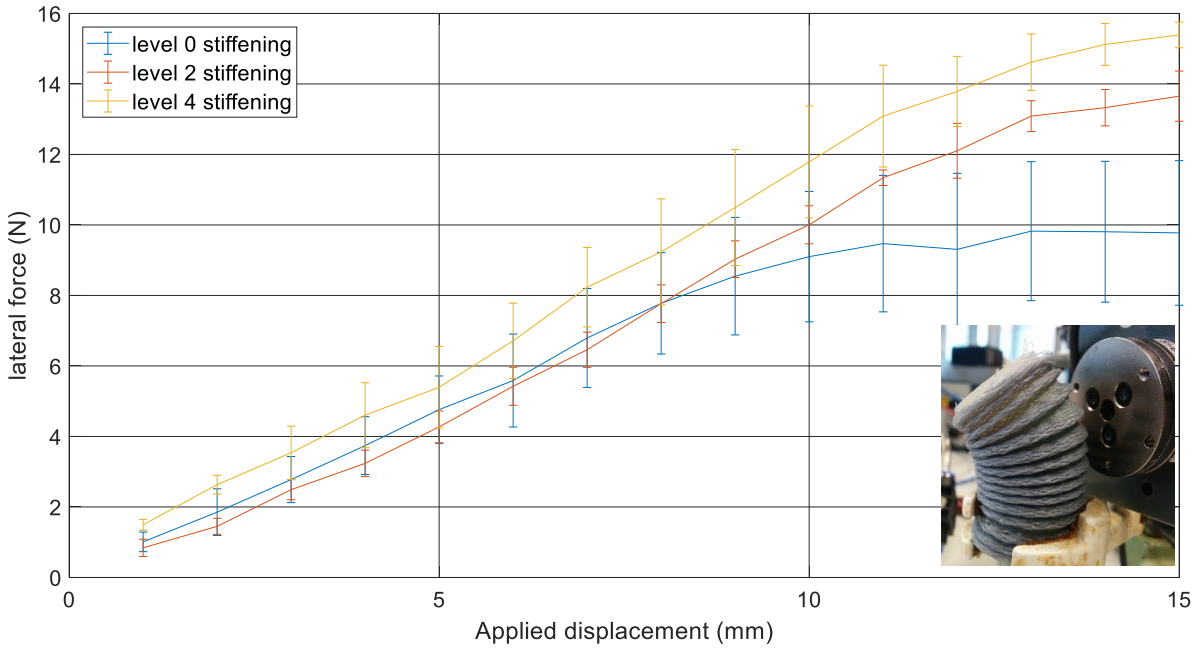

Figure 4.7 Displacement versus applied force for stiffening testing of MOLLUSC manipulator in base condition, (inset) setup of the testing

Results of stiffening experiments in bend condition can be seen in Figure 4.8. For level 1 stiffening, the vacuumed chamber was the one opposite to the chamber activated for bending. In level 2 stiffening, the two stiffened chambers were the chambers in the direction perpendicular to applied force. For level 4 stiffening, the pressurized chamber was quickly switched to vacuum by valve.

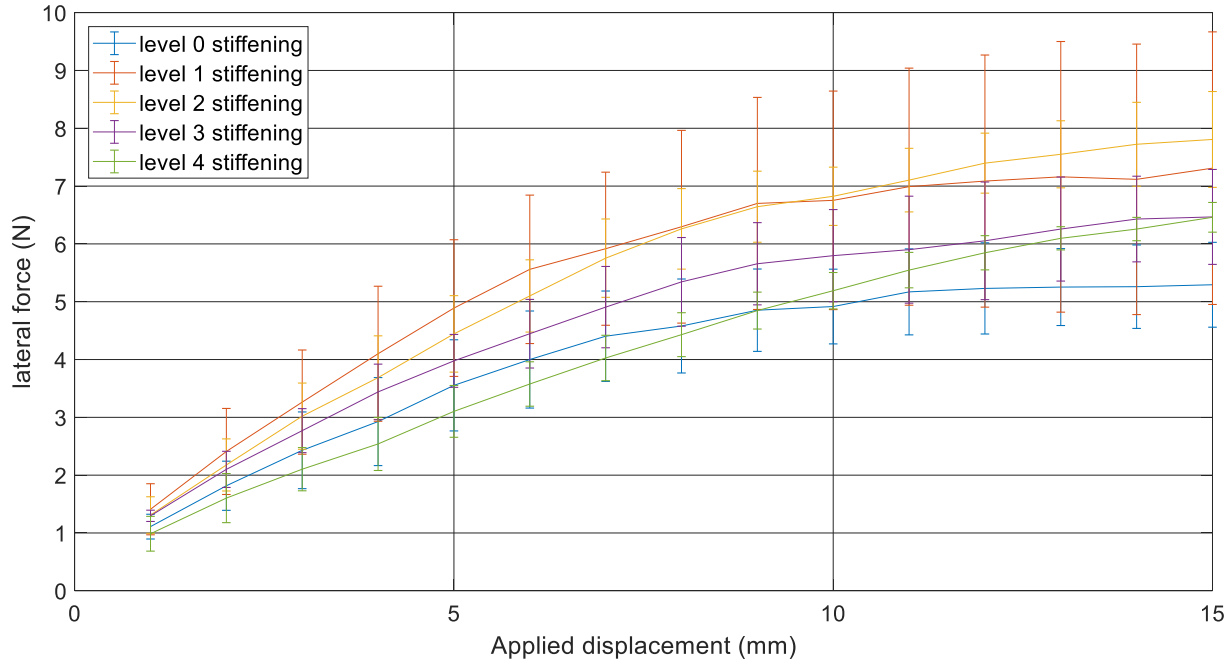

Figure 4.8 Displacement versus applied force stiffening testing of MOLLUSC manipulator in bend condition

4.4. Discussion

4.4.1. Maximum Pressure

The coagulation of coffee powder at the bottom of the chamber can be explained as follow: The air pressure pushes the coffee powder inside the sac to all direction. The pressurized coffee powder may flock at the bottom of the sac due to the gravity. This pressure from the inside of the chamber is countered by relatively stiff material of Ecoflex 50. This pressure from two sides stiffen the coffee powder. When the pressure from inside is bigger than material strength of Ecoflex, then this stiffened coffee powder would slip (and sometime tear) the hole at the bottom of the chamber. To overcome this problem, one solution is to mold another material after the granular jamming sac is inserted. However, with this method, if something happens to the chamber, repairing the chamber is not feasible.

4.4.2. One Chamber Bending

The first curve zone (zero bending angle) is when the air pressure still was filling the chamber. The second zone is when the pressure inside the chamber is enough to bend the actuator. The part of the slow increase in bending angle, as in from pressure of 0.15 bar to 0.25 bar in the module without jamming, is due to free

expansion of the chamber in any direction. The sudden increase in gradient (third curve zone) is due to the friction of chamber with the braided sheath, so the module now is bent into one specific direction [36].

The higher starting pressure of bending in module with jamming is caused by stiffer overall structure due to the neoprene sac and the coffee powder. This stiffer structure also causes the granular jammed module to achieve less bending angle at the same pressure than module without granular jamming. The coffee powder is stiffened at the bottom part of the chamber with the increasing pressure (see Figure 4.1). This stiffened chamber further restricts the chamber bending.

As discussed before, all the curves in bending versus pressure characterization have three zones: a flat, a low gradient and a high gradient zone. For module without jamming, the starting point is lower because the air directly fills the chamber, while in the module with jamming the starting point is higher because first the air needs to fill the granular jamming sac and overcome the added chamber stiffness due to the stretch stiffness of the sac. The transition point between the low gradient and high gradient zones is quite steep in the case of module without jamming material. This transition marked the shift from free expansion of the chamber to the restricted expansion of chamber by the braided sheath [36]. In the case of module with granular jamming, this transition is less steep, and the characteristic curve is more linear than module without jamming. Because the initial pressure needed to expand the granular jamming sac is already quite high (0.3 bar), the restricted expansion by the braided chamber happens at the same time as the chamber expands, thus the behavior of the module is more linear.

4.4.3. Two Chambers Bending

The reduction in bending angle from one to two chambers activation of the module without jamming is 10°. In the module with jamming, bending angle reduction is negligible. This is in contrary with the result reported by Cianchetti et al (2013), where the reduction of bending angle in module without jamming is 40° [36]. As discussed in a later study by Fras et al. (2015), the reduction of bending angle is caused by the cross-section center displacement [35]. As discussed in section 3.2 (Figure 3.3), for the case of three actuation chambers, because the angle between chamber is 120° the resultant vector r1 + r2 (assuming r1= r2) would be r. In our design, the four actuation chambers make the angle between chambers to be 90°, thus the resultant vector r1 + r2 (again assuming r1= r2) would be $r\sqrt{2}$. Furthermore, in case of module with jamming, the stiffness of the other chamber will make it less likely for the cross-section center to be displaced, thus the bending angle curve becomes similar in case one and two chambers bending.

4.4.4. Pressure versus Elongation

In module with jamming, pressurizing all chamber elongated the robot more than pressurizing two chambers by 10-15%. This increase did not occur in module with jamming which means pressurizing all chamber does not increase the elongation. This happens because in module with jamming, when two chambers are pressurized, the two unpressurized chambers would be stiffened because of two sides pressure from activated chamber. This can increase the elongation stiffness of the robot. In activating four chambers, all coffee will be stiff at the bottom of the chambers. The robot body becomes less stiff than in two chambers activation, so it can achieve higher elongation. In the module without jamming, activating all chamber also stiffen all chamber in the same way as activating two chambers stiffen the two chambers. Even though the pressure (and the force) is doubled in the case of four chambers elongation, the stiffness also doubled. Therefore, there is no difference in elongation between two chambers and four chambers activation.

It is noticeable that the shape of the curves resembles the pressure-bending curve of the module without jamming (low gradient followed by higher gradient). This is due to the free expansion of the chambers in the low gradient zone. In the high gradient zone, the module expansion is restricted by the braided sheath, so extra pressure will effectively elongate the robot, thus higher elongation gradient

4.4.5. Pressure versus Force

The result showed that activating more chambers will increase the exerted force. The range of forces is in the range suitable for endoscopic applications mentioned in design specification (refer to section 2.7).

4.4.6. Stiffening Testing

In case of base condition and level 2 stiffening, initially the displacement force was more dominant to bend the silicone rubber rather than bend the stiffened chambers. After the displacement of 10 mm, the reaction force from stiffened chambers became more dominant. In the case of level 4 stiffening, the two activated side chambers (the chambers perpendicular to the direction of applied force) contributed to the reaction force much early from small displacement value. Therefore, the increase in force was observed in all displacements. We can see that vacuuming the chamber increases the stiffness of the module, and two distinct levels of stiffness are attained.

In case of stiffening in bent configuration, the level 1 and level 2 stiffening achieved the same stiffness. Level 2 stiffening gave a higher average value in high displacement (> 10 mm). Level 3 stiffening caused a decrease in stiffening capabilities. This can be explained that in level 3 stiffening, the three activated chambers may decrease the bending angle of the actuated module, hence weaker the stiffness level. In case of level 4 stiffening, the curve is linear, like the curve of level 4 stiffening in base condition (Figure 4.7). This is because in bending level 4, all chambers were vacuumed, this situation was more like base condition with level 4 stiffening. The decrease of stiffness in level 4 stiffening in the region of low displacement (below 8 mm) explains that pressurizing the chamber increase the stiffness of the robot in case of low displacement.

4.5. Conclusion of Experimental Characterization

In this chapter, we performed experimental characterization for MOLLUSC manipulator, which is an improvement from previous STIFF-FLOP design. The improvements aimed to achieve more efficient bending and multi-level stiffness adjustability. The developed module was characterized to describe its mechanical behavior in terms of maximum pressure, bending, elongation, exerted force, and stiffening. For elongation and bending, we compared the behavior of MOLLUSC manipulator with and without granular jamming material. In general, with the insertion of granular jamming sac, we have a design tradeoff. While the stiffness can be adjusted, the module with granular jamming needs higher pressure to achieve the same bending angle/ elongation compared to module without granular jamming. The proposed design improved the bending angle in case of multi chamber bending. The force applied by the module fulfills the surgical requirements. MOLLUSC manipulator is observed to have multi-level stiffness capability.

5. Kinematic Position Control of MOLLUSC Manipulator

5.1. Robot mapping

To simplify the kinematic of MOLLUSC manipulator, we assume that the robot bend in constant curvature fashion. Constant curvature means that all along the central axis the robot has constant radius of curvature (see Figure 5.1 left). This assumption was used in previous pneumatically actuated continuum robot studies, such as Air-Octor and STIFF-FLOP [3], [45].

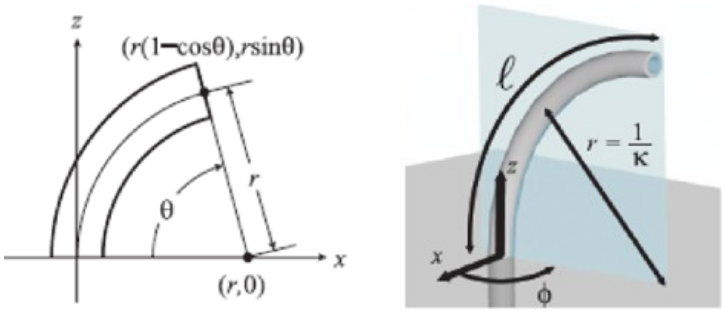

Figure 5.1 (left) constant curvature arc, the origin of curvature is located on (r,0), (right) arc parameter in constant curvature robot, l is the robot backbone length, κ is the curvature of the robot, φ is out-of-plane rotation angle [39]

The kinematic model is based on a review paper by Webster (2010) [39] (Figure 5.2). Under constant kinematic assumption the kinematics can be divided into two mappings. First is the mapping between robot configuration space and task space, we termed them robot independent mapping. The important parameter for continuum robot is the triplet (κ, ϕ, l) which describes robot curvature, out-of-plane angle, and backbone length, respectively (See Figure 5.1 right). The second mapping is the relation between robot specific parameter (chamber length/ chamber pressure) and arc parameter.

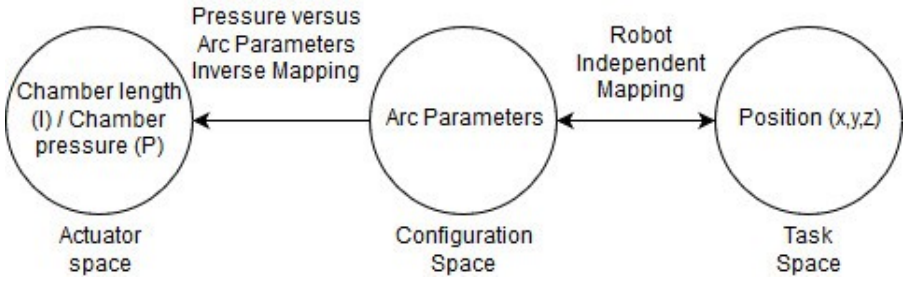

Figure 5.2 Kinematics model of constant curvature continuum robot according to Webster (2010) and customized to model our specific MOLLUSC control algorithm [39]

5.1.1. Robot independent mapping

First, we define the frame convention. We take the positive z-axis tangent to the base of the robot. At $\phi = 0$ the positive bending which results in $\kappa = 0$ happens around the positive y-axis. At $\phi = 0$ if the robot

bend by π radian then the robot will touch the positive x-axis. This frame convention can be seen in Figure 5.1 right.

In Figure 5.1 left, the tip position in the x-z plane without out-of-plane angle is $\boldsymbol{p} = (r(1 - cos\theta), r\ sin\theta)$. This x-z tip position has rotation around the y axis defined by $R_y(\theta) \in SO(3)$. If the in-plane transformation is then multiplied by an out-of-plane rotation around the z-axis defined by $R_z(\phi) \in SO(3)$, a transformation matrix from arc base to tip is obtained [46].

$$T = \begin{bmatrix} R_z(\phi) & 0 \\ 0 & 1 \end{bmatrix} \begin{bmatrix} R_y(\theta) & \boldsymbol{p} \\ 0 & 1 \end{bmatrix}$$

$$T = \begin{bmatrix} cos\phi\cos\theta & -sin\phi & \cos\phi cos\theta & rcos\phi(1-cos\theta) \\ sin\phi\ cos\theta & cos\phi & sin\phi sin\theta & rsin\phi(1-cos\theta) \\ -sin\theta & 0 & \cos\theta & rsin\theta \\ 0 & 0 & 0 & 1 \end{bmatrix} \ldots (1)$$

5.1.2. Robot specific mapping

One way of transformation from arc parameter to robot specific parameter can be done via chamber length. Looking at Figure 5.3 , the length of individual chamber can be derived as in Equation 2 [46]. One important observation is that there will always be chamber(s) that decrease in length if the robot moves.

$$r_i = r - d\ cos\phi_i$$

$$recalling\ that\ l_i = r_i\theta\ and\ l = r\theta$$

$$l = l_i + \theta d\ cos\phi_i$$

$$in\ the\ case\ of\ four\ bending\ chambers, \phi_i = 90 * i - \phi, so$$

$$\begin{bmatrix} l_1 \\ l_2 \\ l_3 \\ l_4 \end{bmatrix} = \begin{bmatrix} l - \theta d\ sin\phi \\ l - \theta d\ cos\phi \\ l + \theta d\ sin\phi \\ l + \theta d\ cos\phi \end{bmatrix} \ldots (2)$$

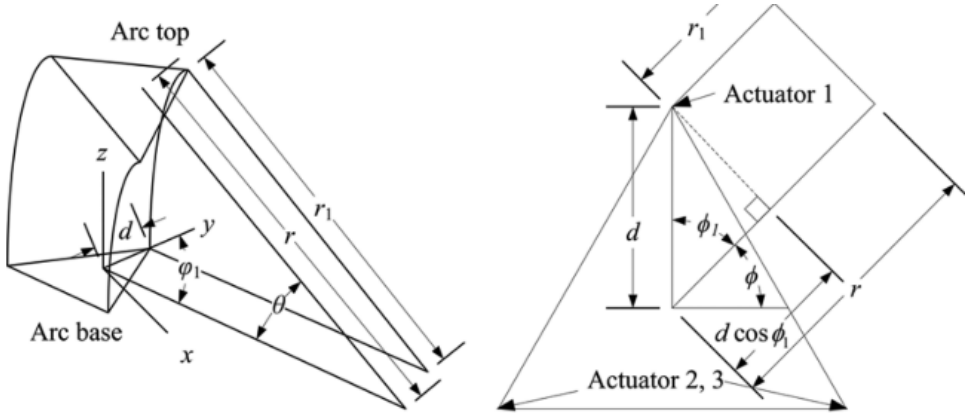

Figure 5.3 (left) schematic of three chambers robot depicting arc parameters of the robot and of chamber r1 (right) schematic of three chambers robot as seen from top, depicting also the arc parameters of the robot and of chamber r1 [39]

5.2. 2D position control of the robot

In the case of MOLLUSC manipulator, pneumatic actuation is used to manipulate the chamber length, therefore we need to find the mapping of pressure versus chamber length. Both the actuated chamber and non-actuated chamber length are measured at pressure of 0 to 0.5 bar with a step of 0.05 bar to obtain the required mapping [47]. The mapping and the curve fitting are presented in Figure 5.4.

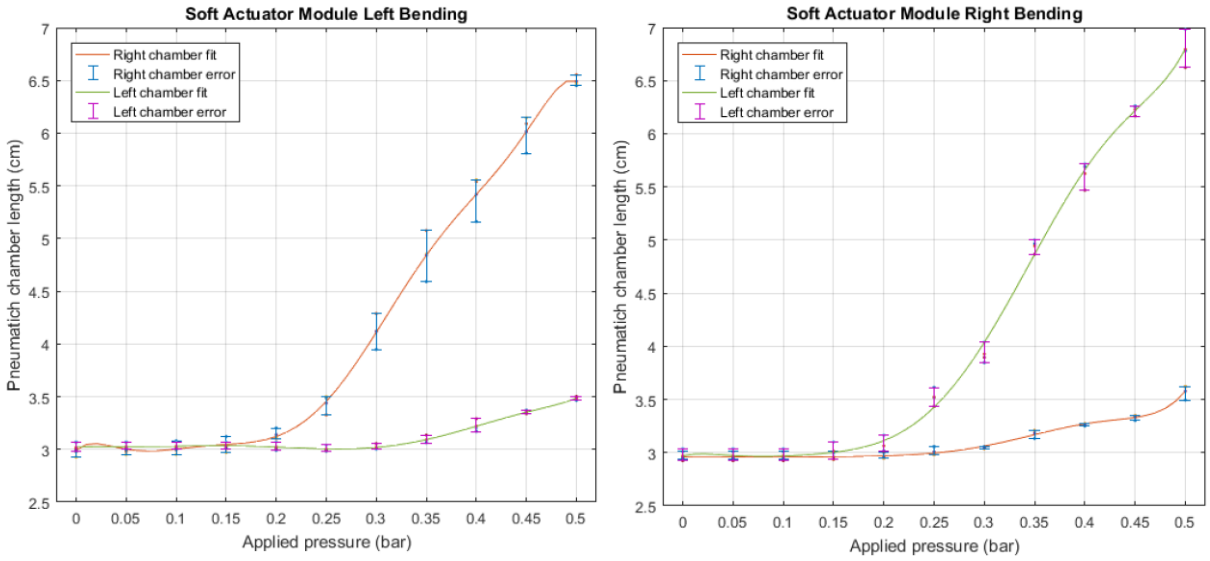

Figure 5.4 The fitting of pressure versus chamber length relationship for right bending of left bending of the module [47]

It is observed that the chamber length of our MOLLUSC manipulator cannot shrink, therefore Equation 3 is modified by assuming that the amount of the chamber shrink will be added to main backbone length instead. The passive chamber length is then assumed to be 3.0 cm (its minimum length) and pressure required to actuate the active chamber is determined. At this amount of pressure, the length of the passive chamber is checked from the curve fitting of the calibration data. If this length is larger than 1% of the calculated passive chamber value, then the new value of passive chamber length will be used to fetch the pressure needed to actuate the active chamber. This iteration will be done until the calibrated passive chamber length is within 1% of the previous iteration value. This algorithm is termed “Passive Chamber Compensation (PCC)” (Figure 5.5) [47].

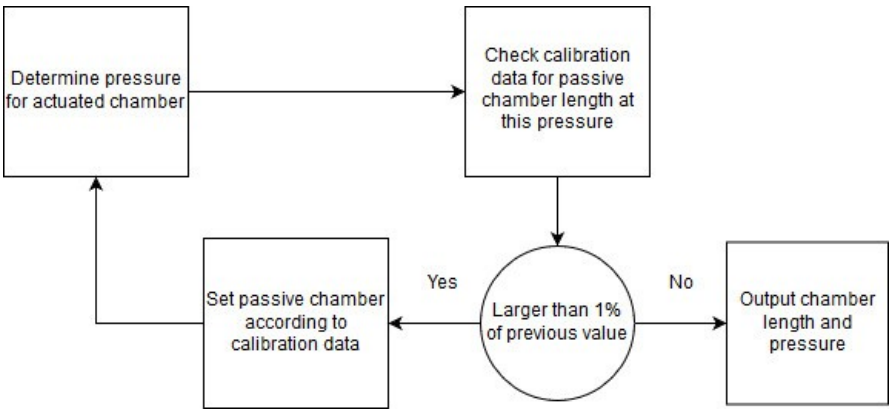

Figure 5.5 Algorithm of passive chamber compensation [47]

Two tests are performed to validate the PCC algorithm by inputting desired angle of 0 to 90° with a step of 15°. One test assumed constant passive chamber length of 3.0 cm, and one test updated the passive chamber length using the PCC algorithm. For right and left bending, PCC gives less error than the algorithm without PCC. The bending angle error of PCC is less than 5° (Figure 5.6).

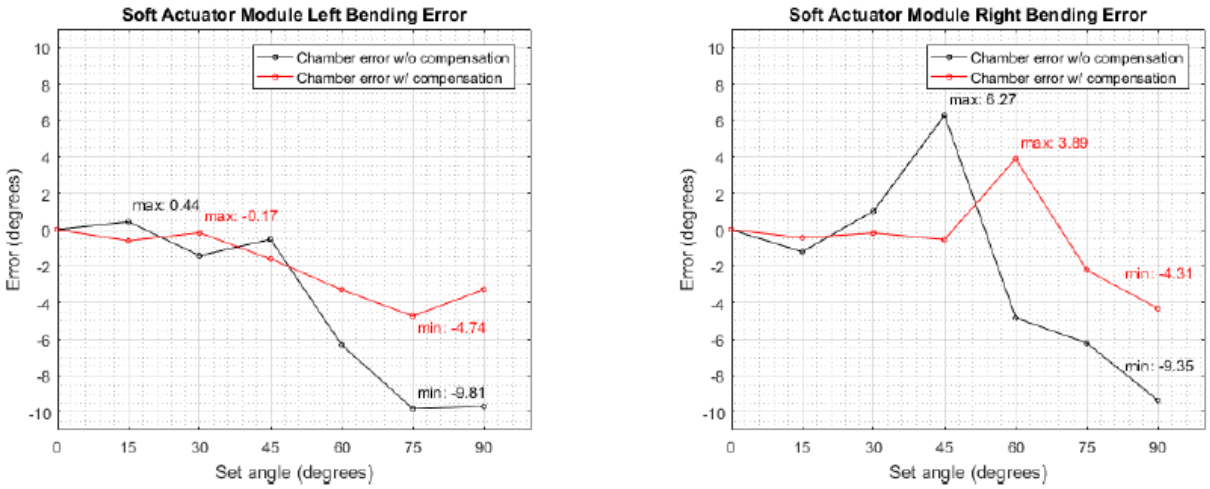

Figure 5.6 (left) Validation result of 2D bending angle control of MOLLUSC manipulator, (left) difference between setpoint and actual bending angle of left bending, (right) difference between setpoint and actual bending angle of right bending [47]

5.3. Simplification and Assumption for 3D Control of the Robot

Jansen (2018) observed that the chamber length cannot shrink below its minimum value [47]. For 2D bending, the length of opposite chamber must be calibrated for more accurate control. In the case of 3D bending, the length of the other three chambers must be calibrated. However, the algorithm will be less simple because with the current manufacture technique we cannot guarantee similar chamber behavior, therefore the three chamber lengths are expected to have different calibration curves.

The triplet of robot configuration is (κ, ϕ, l), but considering the relation $\theta = \kappa * l$ [46], then the triplet can be simplified into tuple (θ, ϕ). In our work, we simplify the 3D control by directly relating pressure to bending angle θ and rotation angle ϕ instead of relating pressure to individual chamber lengths.

Proof of Concept 3D bending by Jansen (2018) concluded that activating two adjacent chambers with the same amount of pressure will move the robot in the ϕ direction of 45°, in addition to also bend the robot [47]. According to the characterization curve in section 3.6.2 (see Figure 4.4), to achieve the same bending angle, activating two chambers needed ±0.025 bar more pressure than activating one chamber. If we assume that pressure difference in the case of actuating one and two chambers simultaneously is negligible, then we can simplify the control algorithm by saying that the pressure needed to bend the robot at specific angle at ϕ =45° is the same as the pressure needed to bend the robot at ϕ =0°.

Based on the assumption that same pressure is needed to activate one chamber and two chambers to achieve the same bending angle, we can have next simplification that bending angle is determined by the chamber with higher pressure (will be called main chamber). To have rotation in the ϕ direction, first we determine which chamber is the main chamber, the orientation of the main chamber ϕ_{main}, and the pressure of the main chamber as function of bending angle $P_{main}(\theta)$. Then we calculate the pressure in the adjacent chamber by calculating the absolute difference of ϕ and ϕ_{main} and apply the formula in Equation 3.

$$P_{adjacent} = P_{main}(\theta) * \tan\big(abs(\phi - \phi_{main})\big) \dots (3)$$

5.4. Implementation of the Control System

For hardware, because we are activating at most two chambers at the same time, we use two pressure regulators with two solenoid valves to control all the four chambers. VEAB series pressure regulator (Festo Inc) and MHE series solenoid valve (Festo Inc) are used to implement the system. Arduino UNO is used as the control board. We activated the valve using TIP120 transistors. Low pass RC filter is used to convert Arduino PWM signal into DC signal to the pressure regulator. The conversion factor between voltage and pressure is deducted from VEAB datasheet.

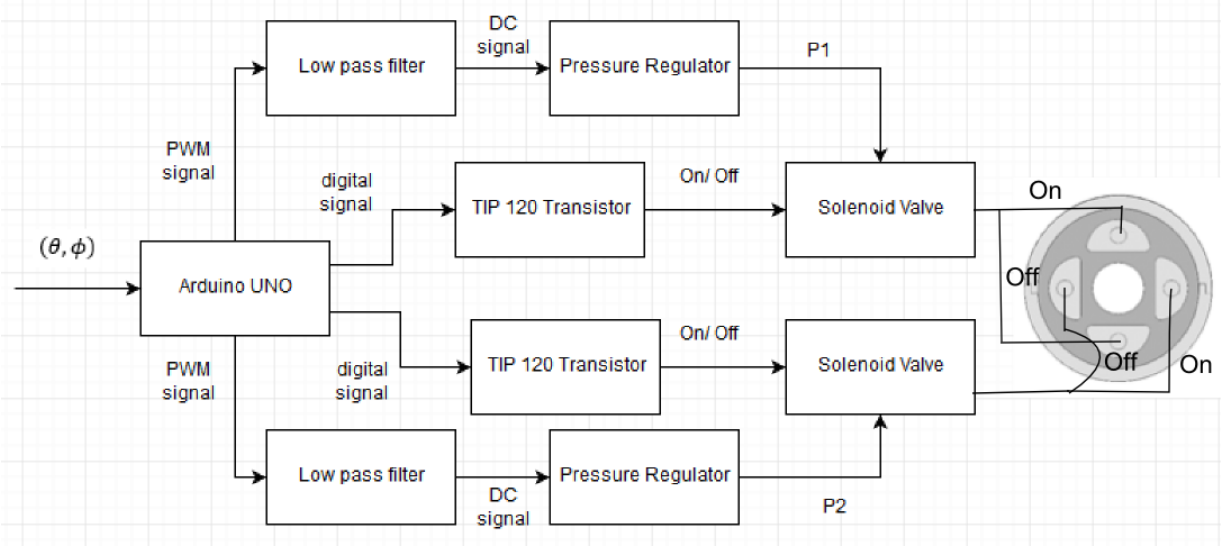

Figure 5.7 implementation of the control system on hardware level. The input signal of θ & ϕ *is sent to Arduino and translated into pressure of the two regulators P1 and P2, and the ON/OFF configuration of the two solenoid valves to choose which chamber(s) to activate*

The algorithm to move robot to specific position can be seen in Figure 5.8. This algorithm is based on simplification and movement strategy described in subsection 5.3. To move the robot along specific trajectory, first the robot is moved to the origin point. Then the robot is moved along azimuthal plane by changing its ϕ by 15° step towards the endpoint ϕ. Lastly, the robot is bent toward the desired final bending angle θ (Figure 5.9).

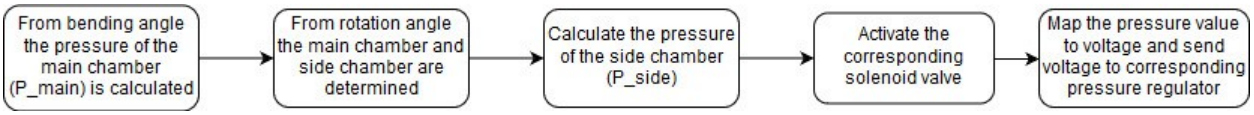

Figure 5.8 algorithm to move the robot to specific bending and rotation angle. The algorithm determines which chamber is the main chamber based on the rotation angle ϕ*. The main chamber pressure P_main is determined by bending angle* θ*. Pressure of the side chamber P_side is determined by tangent of the difference in main chamber and side chamber position* $tan(\mathrm{abs}(\phi - \phi_{\mathrm{main}}))$ *times the pressure of the main chamber P_main*

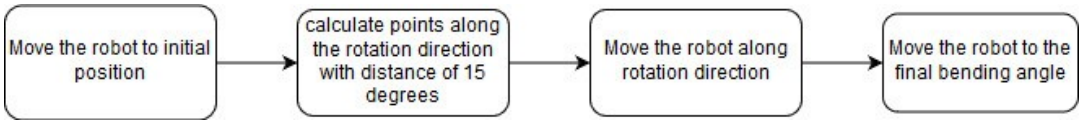

Figure 5.9 algorithm to move the robot between two points. Input to this algorithm is the pair (θ, ϕ) *of the origin point* $(\theta_{\mathrm{ori}}, \phi_{\mathrm{ori}})$ *and the end point* $(\theta_{\mathrm{end}}, \phi_{\mathrm{end}})$*. First, the robot is moved to* $(\theta_{\mathrm{ori}}, \phi_{\mathrm{ori}})$ *then the robot goes from* $(\theta_{\mathrm{ori}}, \phi_{\mathrm{ori}})$ *to* $(\theta_{\mathrm{ori}}, \phi_{\mathrm{end}})$*. Lastly, the algorithm will move the robot from* $(\theta_{\mathrm{ori}}, \phi_{\mathrm{end}})$ *to* $(\theta_{\mathrm{end}}, \phi_{\mathrm{end}})$

5.5. Validation: Static position control

For static position control, we fixed NDI Aurora EM tracker on top of the robot. We also fixed the base to a platform (see Figure 5.10 right). We send command to robot to go to the 90° bending position with $\phi(°) = (0, 30, 45, 60, 90, 120, 135, 150, \ 180)$. $\phi = 0$ is defined to be the bending direction of the right chamber.

For every position, the (x,y,z) position data of the robot is recorded then plotted together with ideal tip position of the robot in the desired angle (θ, ϕ).

To validate the movement of the robot, we need to know the ideal robot tip position if we put input (θ, ϕ). Therefore, we need the robot radius of curvature and the initial tip position of the robot (initial tip position is the same as robot height) to obtain the transformation matrix. The robot curvature is found by bending the robot in 90° and taking the mean of the curvature radius r1 and r2 (see Figure 5.10 left). Robot curvature is calculated to be 46.2 mm. Robot height is measured by ruler, and the value is 50 mm.

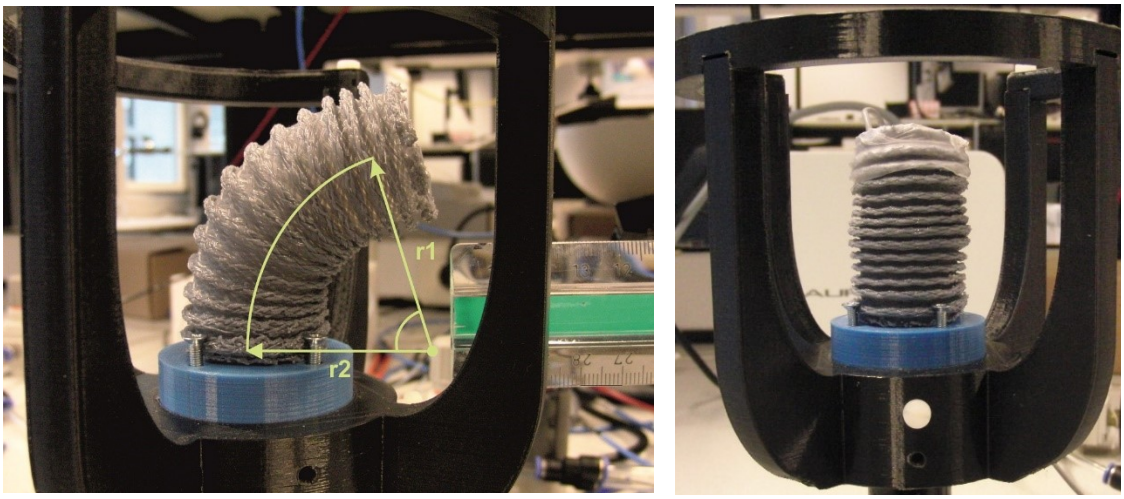

Figure 5.10 (left) determination of robot curvature, robot curvature is calculated by averaging the value of r1 and r2 (right) testing setup for 3D position control of the robot. Aurora tracker is placed in front of the robot

Static position testing reveals that although the robot is given command to bend 90°, the robot bends less than 70° (see Figure 5.11). More careful calibration is nneded for this robot. A few ϕ positions cannot be achieved by the robot, such as ϕ = 60°, 120°, and 150°. The chamber with higher pressure will dictate the phi direction, and with current tangent formula to pressurize the non-dominant chamber (see Equation 3) the resultant phi is only ideal for phi= multiple of 45°. We also see the non-uniform manufacturing in the bending capability of the robot. Bending of the left chamber is less than the front chamber. That is why in the simultaneous bending with the same pressure, the two chambers cannot achieve ϕ =135°.

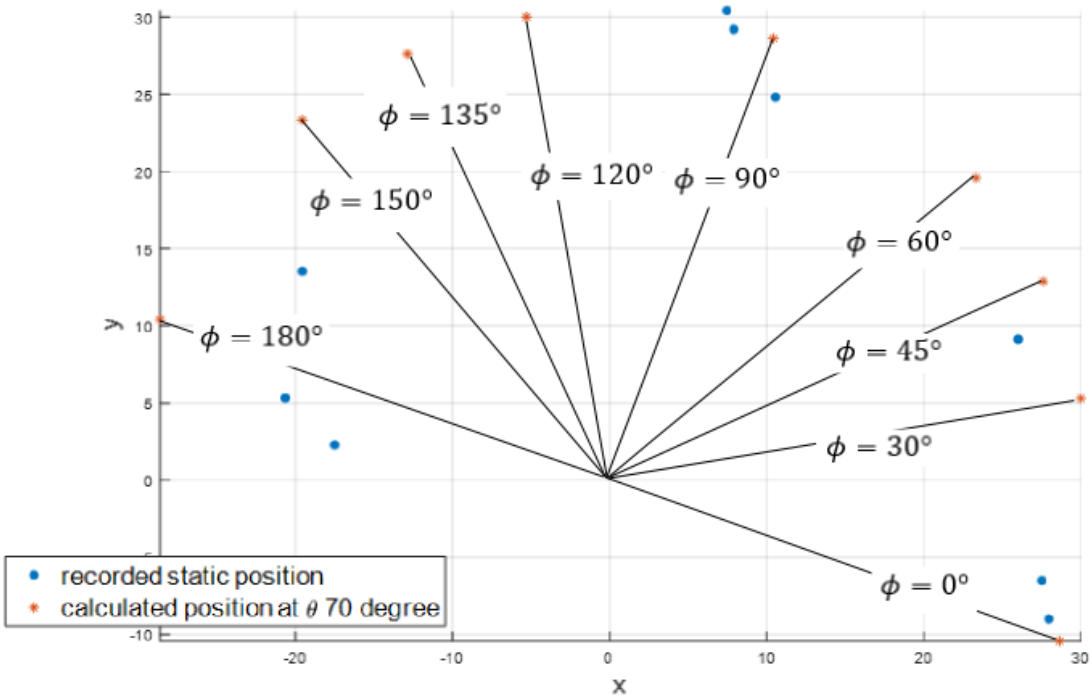

Figure 5.11 Recorded robot position and cacluclated robot position at θ=70 deg bending, as seen from above the X-Y plane.

5.6. Validation: Dynamic position control

For dynamic position control we used the same setup as in section 4.5. However, now the robot is commanded to move in dynamic fashion. For each movement, the sequence is repeated three times. The ideal trajectory is generated using the same transformation as in previous section. Two movements are tested.

1) Move in one quadrant: go from home position to $(\theta, \phi) = (90,0)$ and trace line to $(\theta, \phi) = (90,90)$, go back to home position and repeat the sequence. Home position is defined as $(\theta, \phi) = (0,0)$.
2) Move in full circle: go from home position to $(\theta, \phi) = (90,0)$ and trace full circle with constant θ for three times

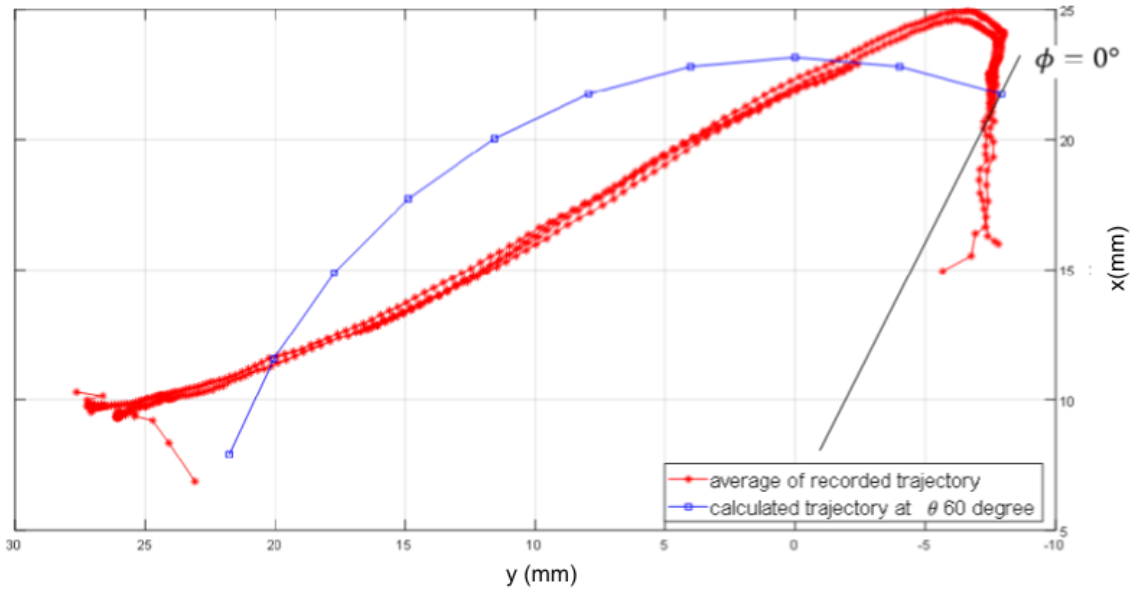

Figure 5.12 robot trajectory compared to ideal trajectory for one quadrant movement as seen from above the X-Y plane. Direction of ϕ=0° is depicted by the black line

From Figure 5.12 we can see that the robot bends at bending angle $\theta = 60°$ instead of 90°. From ϕ perspective, the robot can trace the trajectory desired, although not in exact circular fashion. From static testing position, we see that there are several positions that are not achievable by the robot. However, that is not the case with dynamic positioning. Robot can trace dynamic trajectory due to the fact that air needs some time to be emptied from the chambers (similar to what a capacitor does in RC filter), and by varying the chamber pressure quickly, it is possible to move the robot along specific trajectory.

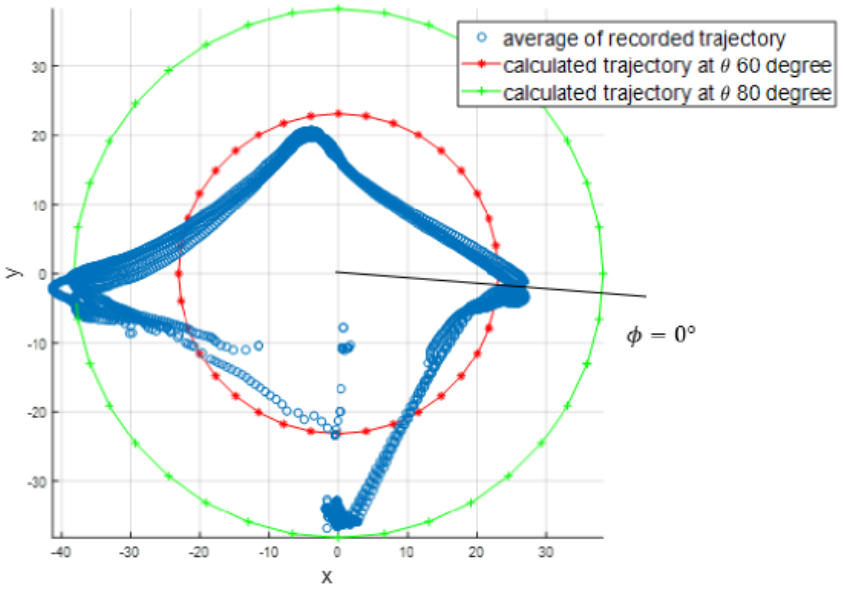

Figure 5.13 robot trajectory compared to ideal trajectory for full circle movement as seen from above the X-Y plane. Direction of ϕ=0° is depicted by the black line. X and Y are expressed in mm.

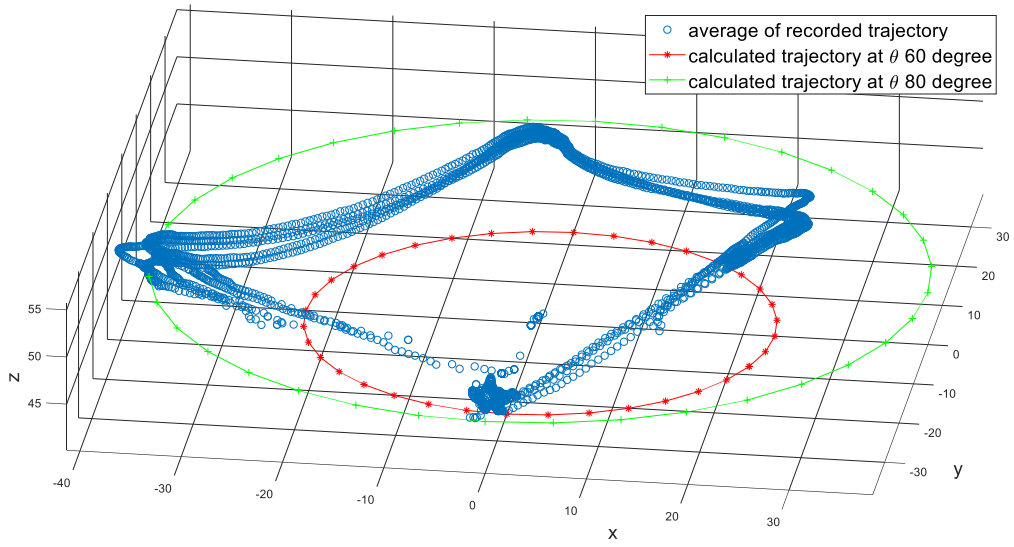

Figure 5.14 robot trajectory compared to ideal trajectory for full circle movement, (right) error in θ and ϕ direction. X and Y are expressed in mm.

From Figure 5.13 and Figure 5.14 we can see that the robot traces trajectory more in square fashion than in circular fashion. The fact that not all bending angle are equal, due to non-uniform manufacturing can be seen by the achievable bending angle at $\phi = 0°, 90°, 180°, \& 270°$. Another noticeable property is the less bending angle when two chambers are pressurized together. The robot retracts slightly along its trajectory.

5.7. Conclusion of kinematic control of the robot

2D control of the robot can be achieved with bending angle error less than 5° using the passive chamber compensation algorithm designed by Jansen (2018) [47]. 3D control of the robot is more challenging due to more complex calibration. To record chamber lengths in various θ and ϕ and map the pressure to the four chamber lengths require multi-dimensional interpolation which is computationally heavy. One simplification that is tested in our control strategy assumes that the bending angle is determined by the main chamber, and the ϕ is governed by main and adjacent chamber that is pressurized according to tangential relationship.

Proof of concept in static testing reveal that for static 3D positioning, our algorithm works accurately only for φ multiple of 45°. For static position testing, another algorithm should be explored. However, in dynamic trajectory motion of the robot, our algorithm can achieve the quadrant and circular trajectory, although not perfectly circular. Because pressurized chamber needs time to be relaxed, trajectory tracing is possible in the case of dynamic control.

6. Conclusion & Future Direction

6.1. Conclusion

This study aimed to design new soft surgical endoscope that fulfill four crucial capabilities mentioned in the introduction: **stiffness adjustment, bendability, controllability,** and **trackability.**

Novel design concept based on STIFF-FLOP design, termed MOLLUSC manipulator, has been manufactured and characterized. To be safe pressure from pressure leakage and chamber explosion, the pressure must be kept below 0.75 bar. In term of **stiffness adjustment,** this novel design can achieve up to four stiffness levels in one chamber bending scenario with stiffness variation ranging from 20 to 40%. In the base condition, the stiffness can increase up to 57%. In term of **bendability** the version without jamming material can bend to 80° at pressure of 0.45 bar, and version with jamming material can bend to 50°. MOLLUSC design with jamming material enhance the stiffness adjustment but at the cost of reducing the bendability. In case of multi chamber bending, four chambers MOLLUSC achieve higher bending angle than three chambers STIFF-FLOP. In addition, the proposed MOLLUSC design can deliver force up to 18.88 N and has a central free lumen with a diameter of 6mm that can house endoscopic camera and surgical tools.

In term of **controllability,** open-loop 2D control using chamber length as robot specific parameter has been implemented and improved with PCC algorithm, and the resulting error is less than 5°. In our work, we developed simplified control method for 3D control which determine the pressure of main chamber and deduce the pressure of adjacent chamber by tangential relationship. Static position testing of this algorithm showed that the robot can achieve ϕ multiple of 45°. For other ϕ position, the static 3D control is far than accurate. For the case of dynamic control, time delay caused by the time needed for air to enter or escape the chamber enable robot movement along predefined trajectory. For circular movement tried, the trajectory resembles rhombus more than a circle.

So far, no electromagnetic components are present in the MOLLUSC design. Theoretically, the robot is MR compatible. Therefore, the **trackability** is achieved by MR-imaging. The robot can be tested inside MRI and closed-loop control system can be developed based on the tip kinematics measured from the MR images.

6.2. Future direction

To obtain the best dimension of the robot, finite element simulation should be done before the manufacture phase. Mechanical characterization results from this report can inform initial design of the manipulator. Then, tuning of the dimension and parameter of the robot will predict the behavior of the robot. In the next design, the predicted model behavior should be compared with the actual robot.

There are granular jamming parameters that can be varied: weight of coffee, membrane material and initial length/ shape of the membrane. It is also possible to vary the coarseness of the coffee used. Further experiment should explore how those parameters affect the behavior of the robot. Seeing how those parameters interact, we can obtain the best settings for specific application. The problem with granular jamming sac is they are not uniformly distributed along the chamber. One obstacle that happen with the coffee powder is they tend to flock at the bottom of the chamber because of gravity. A beehive like structure from flexible filter material will ensure uniform distribution of coffee throughout the experiment. Another improvement for the granular jamming is the fixation of the sac to the upper part of the chamber. This

fixation will ensure more uniform stiffening behavior in the vertical direction, thus uniformly stiffen the MOLLUSC robot along its length.

The tradeoff between bending and stiffness in MOLLUSC can be useful for different application. For example, in three segments MOLLUSC robot, it is better for tip segment to use granular jamming sac to achieve more stiffness, while in middle and proximal segment, it is better to use MOLLUSC robot without jamming to achieve better bending capability. With multi-level stiffening in antagonistic pair, theoretically it is possible to modulate force in specific pose. In our work we managed to control the position, however force control is not yet implemented. Future work should implement and validate the force control system.

Based on my current design (MOLLUSC), two parallel projects within Soft Robotics research at Robotics and Mechatronics lab (RaM), university of Twente, to integrate the endoscopic module are running, as explained in the following:

- Willem Hoitzing explored the use of strain gauge to detect external force applied to the endoscope. Furthermore, the force sensor is integrated with phantom omni robotic arm to achieve haptic feedback. In application, the phantom omni will move stiffer when the endoscope starts to interact with external object. This will enhance the safety of the endoscope. However, we must also quantify the interference by the strain gauge with MR-imaging, whether it is still on acceptable level.

- Jorn Jansen has developed control algorithm for multi-segments module. Integration and testing of multi segments module, together with haptic feedback, will bring the robot closer to clinical application. In the physical realization of multi-segments module, the routing of the tubing must be designed carefully. Finally, with the miniaturization of the robot in multi-segments design, hopefully the robot can be closer to application in NOTES procedure.

References

[1] “Laparoscopy.” [Online]. Available: http://www.dishafertility.com/laparoscopy.html.

[2] “Endoscope.” [Online]. Available: https://accessmedicine.mhmedical.com/Content.aspx?bookId=980&sectionId=59610855.

[3] H. Abidi *et al.*, “Highly dexterous 2-module soft robot for intra-organ navigation in minimally invasive surgery,” *Int. J. Med. Robot. Comput. Assist. Surg.*, vol. 14, no. 1, pp. 1–9, 2018.

[4] M. Cianchetti and A. Menciassi, “Soft Robots in Surgery,” in *Soft Robotics: Trends, Applications and Challenges*, vol. 17, 2017, pp. 78–88.

[5] N. Kurniawan and M. Keuchel, “Flexible Gastro-intestinal Endoscopy — Clinical Challenges and Technical Achievements,” *Computational and Structural Biotechnology Journal*. 2017.

[6] S. Atallah, B. Martin-Perez, D. Keller, J. Burke, and L. Hunter, “Natural-orifice transluminal endoscopic surgery,” *Br. J. Surg.*, vol. 102, no. 2, pp. 73–92, 2015.

[7] R. G. Beckett, “Application and Limitations of Endoscopy in Anthropological and Archaeological Research,” *Anat. Rec.*, 2015.

[8] H. J. Marcus, T. P. Cundy, A. Hughes-Hallett, G. Z. Yang, A. Darzi, and D. Nandi, “Endoscopic and keyhole endoscope-assisted neurosurgical approaches: A qualitative survey on technical challenges and technological solutions,” *Br. J. Neurosurg.*, vol. 28, no. 5, pp. 606–610, 2014.

[9] M. Cianchetti and A. Menciassi, *Soft Robotics: Trends, Applications and Challenges*, vol. 17. 2017.

[10] S. Kim, C. Laschi, and B. Trimmer, “Soft robotics: A bioinspired evolution in robotics,” *Trends Biotechnol.*, vol. 31, no. 5, pp. 287–294, 2013.

[11] D. Rus and M. T. Tolley, “Design, fabrication and control of soft robots,” *Nature*, vol. 521, no. 7553, pp. 467–475, 2015.

[12] M. Manti, V. Cacucciolo, and M. Cianchetti, “Stiffening in soft robotics: A review of the state of the art,” *IEEE Robot. Autom. Mag.*, vol. 23, no. 3, pp. 93–106, 2016.

[13] P. Polygerinos *et al.*, “Soft Robotics: Review of Fluid-Driven Intrinsically Soft Devices; Manufacturing, Sensing, Control, and Applications in Human-Robot Interaction,” *Adv. Eng. Mater.*, vol. 19, no. 12, 2017.

[14] B. Davies, “A review of robotics in surgery,” *Proc. Inst. Mech. Eng. Part H J. Eng. Med.*, vol. 214, no. 1, pp. 129–140, Jan. 2000.

[15] H. Elhawary, A. Zivanovic, B. Davies, and M. Lampérth, “A Review of Magnetic Resonance Imaging Compatible Manipulators in Surgery,” *Proc. Inst. Mech. Eng. Part H J. Eng. Med.*, vol. 220, no. 3, pp. 413–424, Mar. 2006.

[16] W. Yao and P. R. Childs, “Application of design rationale for a robotic system for single-incision laparoscopic surgery and natural orifice transluminal endoscopic surgery,” *Proc. Inst. Mech. Eng. Part H J. Eng. Med.*, vol. 227, no. 7, pp. 821–830, Jul. 2013.

[17] G. Dogangil, B. L. Davies, and F. Rodriguez y Baena, “A review of medical robotics for minimally invasive soft tissue surgery,” *Proc. Inst. Mech. Eng. Part H J. Eng. Med.*, vol. 224, no. 5, pp. 653–

679, May 2010.

[18] M. Li *et al.*, "Intra-operative tumour localisation in robot-assisted minimally invasive surgery: A review," *Proc. Inst. Mech. Eng. Part H J. Eng. Med.*, vol. 228, no. 5, pp. 509–522, May 2014.

[19] D. Chen and Q. Pei, "Electronic Muscles and Skins: A Review of Soft Sensors and Actuators," *Chem. Rev.*, vol. 117, no. 17, pp. 11239–11268, Sep. 2017.

[20] A. Miriyev, K. Stack, and H. Lipson, "Soft material for soft actuators," *Nat. Commun.*, vol. 8, no. 1, p. 596, Dec. 2017.

[21] Y. Kim, S. S. Cheng, M. Diakite, R. P. Gullapalli, J. M. Simard, and J. P. Desai, "Toward the Development of a Flexible Mesoscale MRI-Compatible Neurosurgical Continuum Robot," *IEEE Trans. Robot.*, vol. 33, no. 6, pp. 1386–1397, 2017.

[22] M. Cianchetti *et al.*, "Soft Robotics Technologies to Address Shortcomings in Today's Minimally Invasive Surgery: The STIFF-FLOP Approach," *Soft Robot.*, vol. 1, no. 2, pp. 122–131, 2014.

[23] B. S. Peters, P. R. Armijo, C. Krause, S. A. Choudhury, and D. Oleynikov, "Review of emerging surgical robotic technology," *Surgical Endoscopy and Other Interventional Techniques*. 2018.

[24] J. E. Bernth, A. Arezzo, and H. Liu, "A Novel Robotic Meshworm with Segment-Bending Anchoring for Colonoscopy," *IEEE Robot. Autom. Lett.*, vol. 2, no. 3, pp. 1–1, 2017.

[25] A. D. Marchese, R. K. Katzschmann, and D. Rus, "A Recipe for Soft Fluidic Elastomer Robots," *Soft Robot.*, vol. 2, no. 1, pp. 7–25, 2015.

[26] S. Kim, E. Hawkes, K. Cho, M. Jolda, J. Foley, and R. Wood, "Micro artificial muscle fiber using NiTi spring for soft robotics," in *2009 IEEE/RSJ International Conference on Intelligent Robots and Systems, IROS 2009*, 2009, pp. 2228–2234.

[27] Ching-Ping Chou and B. Hannaford, "Measurement and modeling of McKibben pneumatic artificial muscles," *IEEE Trans. Robot. Autom.*, vol. 12, no. 1, pp. 90–102, 1996.

[28] J. Bishop-Moser, G. Krishnan, C. Kim, and S. Kota, "Design of soft robotic actuators using fluid-filled fiber-reinforced elastomeric enclosures in parallel combinations," *IEEE Int. Conf. Intell. Robot. Syst.*, pp. 4264–4269, 2012.

[29] S. Ozel *et al.*, "A composite soft bending actuation module with integrated curvature sensing," *Proc. - IEEE Int. Conf. Robot. Autom.*, vol. 2016–June, pp. 4963–4968, 2016.

[30] H. Zhao, R. Huang, and R. F. Shepherd, "Curvature control of soft orthotics via low cost solid-state optics," *Proc. - IEEE Int. Conf. Robot. Autom.*, vol. 2016–June, pp. 4008–4013, 2016.

[31] S. Groth, D. K. Rex, T. Rösch, and N. Hoepffner, "High cecal intubation rates with a new computer-assisted colonoscope: A feasibility study," *Am. J. Gastroenterol.*, 2011.

[32] A. Eickhoff *et al.*, "Computer-assisted colonoscopy (the NeoGuide Endoscopy System): Results of the first human clinical trial ('PACE Study')," *Am. J. Gastroenterol.*, 2007.

[33] A. Gudeloglu, J. V Brahmbhatt, and S. J. Parekattil, "Robotic microsurgery in male infertility and urology-taking robotics to the next level," *Transl Androl Urol*, 2014.

[34] M. Cianchetti *et al.*, "Soft Robotics Technologies to Address Shortcomings in Today's Minimally Invasive Surgery: The STIFF-FLOP Approach," *Soft Robot.*, vol. 1, no. 2, pp. 122–131, 2014.

[35] J. Fras, J. Czarnowski, M. Macias, J. Glowka, M. Cianchetti, and A. Menciassi, “New STIFF-FLOP module construction idea for improved actuation and sensing,” *Proc. - IEEE Int. Conf. Robot. Autom.*, vol. 2015–June, no. June, pp. 2901–2906, 2015.

[36] M. Cianchetti, T. Ranzani, G. Gerboni, I. De Falco, C. Laschi, and A. Menciassi, “STIFF-FLOP surgical manipulator: Mechanical design and experimental characterization of the single module,” in *IEEE International Conference on Intelligent Robots and Systems*, 2013.

[37] B. Yang, U. X. Tan, A. B. McMillan, R. Gullapalli, and J. P. Desai, “Design and control of a 1-DOF MRI-compatible pneumatically actuated robot with long transmission lines,” *IEEE/ASME Trans. Mechatronics*, 2011.

[38] B. A. Jones and I. D. Walker, “Kinematics for multisection continuum robots,” *IEEE Trans. Robot.*, 2006.

[39] R. J. Webster and B. A. Jones, “Design and kinematic modeling of constant curvature continuum robots: A review,” *Int. J. Rob. Res.*, 2010.

[40] K. Althoefer, “Antagonistic actuation and stiffness control in soft inflatable robots,” *Nat. Rev. Mater.*, vol. 3, no. June, pp. 1–2, 2018.

[41] N. G. Cheng *et al.*, “Design and Analysis of a Robust, Low -cost , Highly Articulated Manipulator Enabled by Jamming of Granular Media,” *Proc. 2012 IEEE Int. Conf. Robot. Autom.*, pp. 4328–4333, 2012.

[42] A. Jiang *et al.*, “Robotic Granular Jamming: Does the Membrane Matter?,” *Soft Robot.*, vol. 1, no. 3, pp. 192–201, 2014.

[43] “Module Fabrication.” [Online]. Available: https://softroboticstoolkit.com/mmvsm/fabrication/modules.

[44] “Braided Sheath.” [Online]. Available: https://softroboticstoolkit.com/mmvsm/fabrication/braided-sheath.

[45] W. McMahan, B. A. Jones, and I. D. Walker, “Design and implementation of a multi-section continuum robot: Air-octor,” *2005 IEEE/RSJ Int. Conf. Intell. Robot. Syst. IROS*, pp. 3345–3352, 2005.

[46] R. J. Webster and B. A. Jones, “Design and kinematic modeling of constant curvature continuum robots: A review,” *Int. J. Rob. Res.*, vol. 29, no. 13, pp. 1661–1683, 2010.

[47] J. Jansen, “Endoscopic end effector control using soft actuator,” *Bachelor Thesis RAM*, vol. June, 2018.

[48] B. Mosadegh *et al.*, “Pneumatic networks for soft robotics that actuate rapidly,” *Adv. Funct. Mater.*, vol. 24, no. 15, pp. 2163–2170, 2014.

[49] P. Polygerinos *et al.*, “Towards a soft pneumatic glove for hand rehabilitation,” *IEEE Int. Conf. Intell. Robot. Syst.*, pp. 1512–1517, 2013.

[50] “Pneunet Design.” [Online]. Available: https://softroboticstoolkit.com/book/pneunets-design.

[51] F. Ilievski, A. D. Mazzeo, R. F. Shepherd, X. Chen, and G. M. Whitesides, “Soft robotics for chemists,” *Angew. Chemie - Int. Ed.*, vol. 50, no. 8, pp. 1890–1895, 2011.

[52] “Pneunet Step 3.” [Online]. Available: https://softroboticstoolkit.com/book/pneunets-step-3.

[53] “Pneunet Step 4.” [Online]. Available: https://softroboticstoolkit.com/book/pneunets-step-4.

[54] I. De Falco, A. Menciassi, and M. Cianchetti, “Stiff-flop surgical manipulator: design and preliminary motion evalutaion,” *4th Jt. Work. New Technol. Comput. Assist. Surg.*, no. October 2014, pp. 131–134, 2014.

Appendices

A. First Design Study – Antagonistic Pneu-net

A.1. Design Overview

To address design specifications mentioned in previous chapter, in this chapter, a specific design idea, based on a developed pneu-net actuator[48] antagonistically arranged inside a flexible tube will be pursued. Pneunet is comprised of connected chambers that is constrained by inextensible layer (for example paper) at the bottom part (see Figure A.1) [49]. The repulsion between the chambers will make the actuator bends (see Figure A.1). The pneu-net design is volume efficient, therefore it is useful to design compact robot such as in our case.

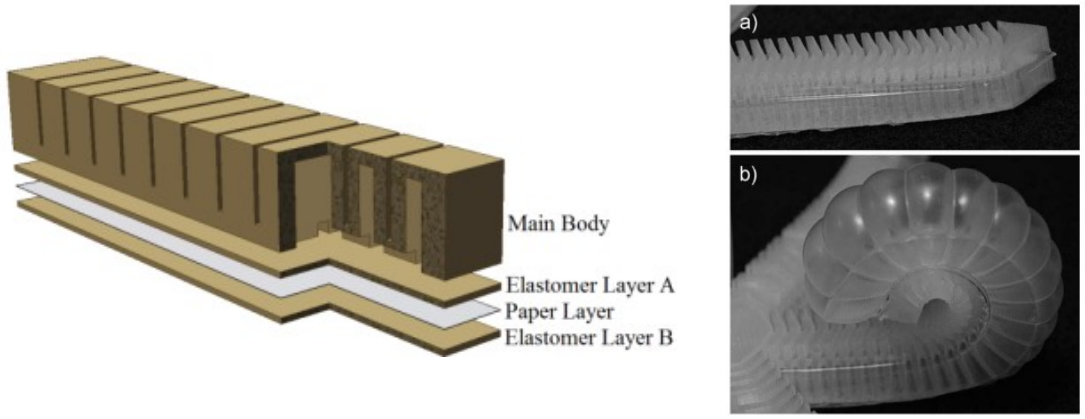

Figure A.1 (left) structure of pneu-net actuator [50]*, (right) a) manufactured pneu-net actuator, b) bending of pneu-net* [51]

In our design, the pneu-net actuator will be arranged antagonistically. Antagonistic actuation strategy is used in many organism, one example is human bicep and triceps. By antagonistic actuation, it is possible to achieve the co-contraction, which mean we can modulate the force exerted and joint stiffness in one specific configuration. In addition, antagonistically arranged chambers would allow precise exerted force and complicated motion trajectories [40]. To achieve the modular continuum design, the antagonistically arranged pneu-net actuator will be embedded inside a modular tube (Figure A.2). The tube should be made from soft and flexible material.

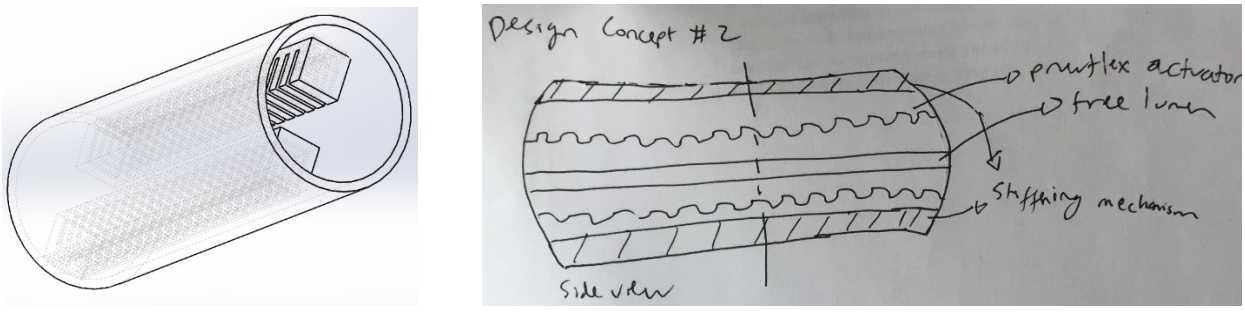

Figure A.2 Design overview of soft endoscopic robots using antagonistic pneu-net actuator, (right) solidworks image, (left) concept drawing

A.2. Method of Manufacturing

One of the challenges in soft robotics implementation is its manufacture. In the beginning, we tried to manufacture directly the pneu-net actuator by 3d printing using Tangoblack Material (Stratasys). Tango black is a flexible material that can bent easily. However, the 3d printed pneu-net actuator did not have good durability. In some part, the actuator ruptured (Figure A.3). We then switched to molding and curing technique to manufacture the actuator.

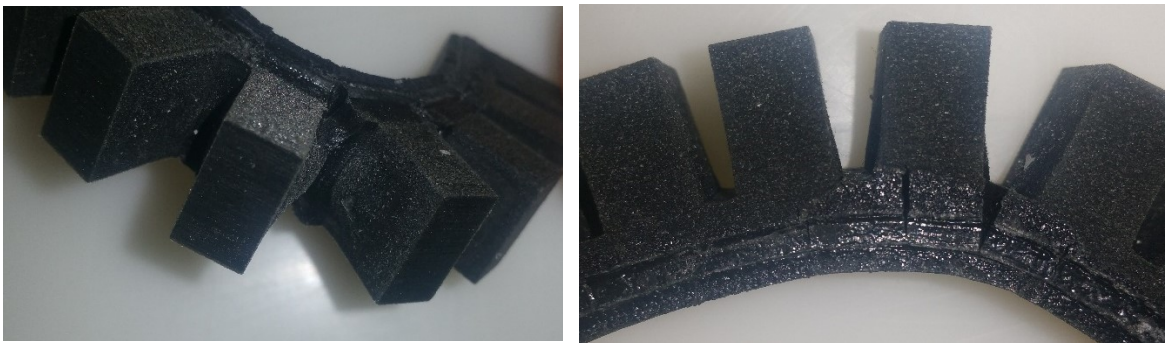

Figure A.3 (left) rupture in the 3d-printed pneu-net actuator

First, the mold of the actuator needs to be manufactured. There are several materials possible for making the mold using 3D printer, such as PLA, ABS, or Verowhite (Verowhite, Stratasys). The mold made from PLA is very sticky when the material already cured. The mold from ABS needs smoothing on the surface using acetone. The mold from Verowhite can be used without stickiness from the cured material. Hence, the used mold for the production is made either from ABS or Verowhite. There are three parts of the mold. Two molds used for producing the upper part and one mold to produce the bottom part (Figure A.4 a and b).

After the mold is printed, then we pour the molding material, which in our case we use Dragonskin 10 (Dragonskin, Smooth-on). The dragon skin first needs to be mixed in 1:1 ratio between part A and part B. We the applied vacuum to remove the bubbles. We then poured the mold into the upper part and half of the bottom part and wait until the material cured. After that, we pour elastomer to the bottom mold. A piece of paper (the inextensible material) is cut and dip it into the liquid bottom mold. We removed the cure upper part from the mold. Then this upper part is pushed a little bit to the liquid bottom part (Figure A.4 c), and after that we wait until the whole structure is cured.

To insert the tubing, first we need to make small hole in the actuator in the direction as shown in Figure A.4 d. To ensure that the tubes are connected, the needle can also be pierced toward the other end of the actuator. Care need to be taken not to pierce the actuator walls. Finally, we inserted the tube that has been layered with superglue to seal the air.

After finishing the actuator, the next challenge is to make the flexible tube. We tried several approaches to make the flexible tube. First, we directly manufacture the tube using the same mold material (Dragonskin 10). Next alternative, we tried to glue the actuator inside a flexible gardening hose and washing machine hose.

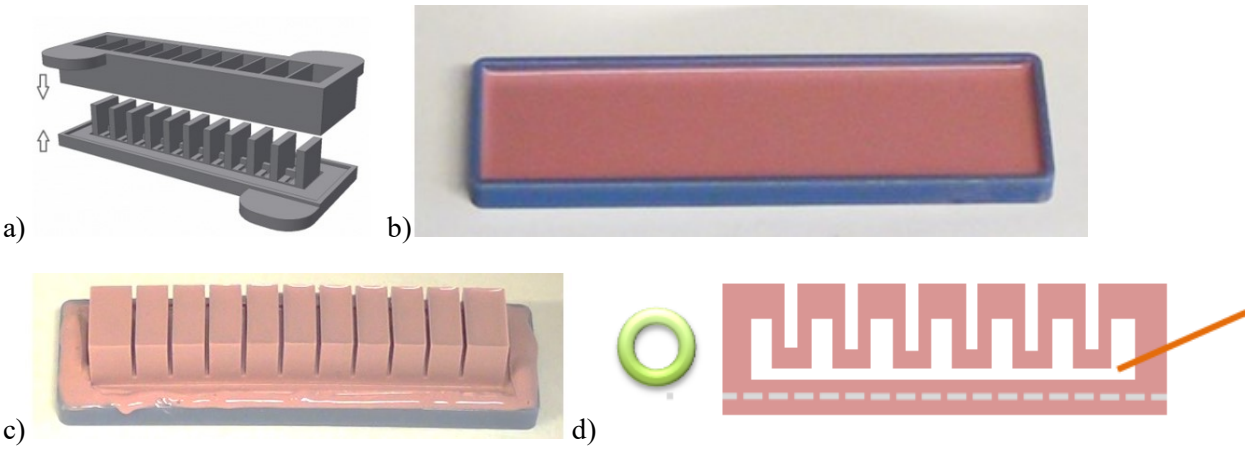

Figure A.4 (a) mold to produce the upper part of the pneu-net [50] *(b) mold to produce the bottom part of the pneu-net* [50] *(c) the cured upper part is dip into uncured bottom part* [52] *(d) direction to pierce the actuator for the tubing hole* [53]

A.3. Low-level Control System

The input for the control system will be the bending angle, stiffness level, and the bending direction (see Figure A.5). If we have the pressure versus bending angle characteristic, then we can obtain the pressure necessary to produce certain angle. This pressure can be subsequently translated into the required voltage that will be fetch to the pressure regulator. Actuating the two regulators at different pressure, we can also modulate the stiffness of the actuator.

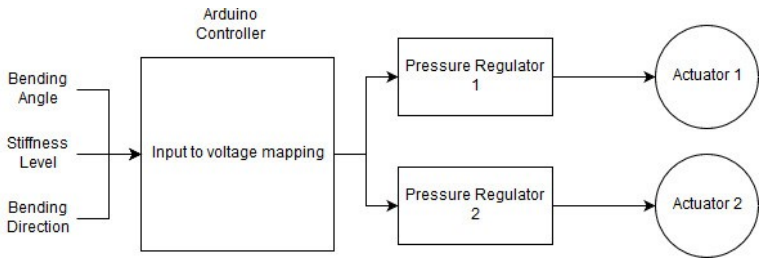

Figure A.5 low-level control for the proposed design

A.4. Experimental Characterization: Bending testing

The testing is setup as in Figure A.6 left. We used manual pressure regulator (AR20-F02-1N-B, SMC) to fetch the air into the actuator. The platform is made of 3D printed PLA structure. A measurement camera is mounted on the tripod that is placed directly in front of the testing setup. The actuator is fixed in one end of the platform. Based from the image of the actuator, the bending angle is measured by calculating the angle between orthogonal line at the tip and at the base of the manipulator [54]. In the measurement example of Figure A.6, it is the angle referred by the curved yellow line.

Based on the curve we obtained, the actuator behavior is non-linear (Figure A.6 right). This can be explained by the existence of paper as the inextensible layer. At the pressure below 1 bar, the bending is restrained by the paper. At pressure higher than 1 bar, the bending becomes easier with higher gradient.

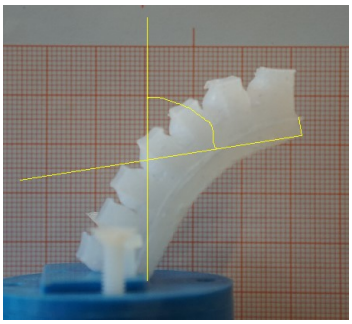

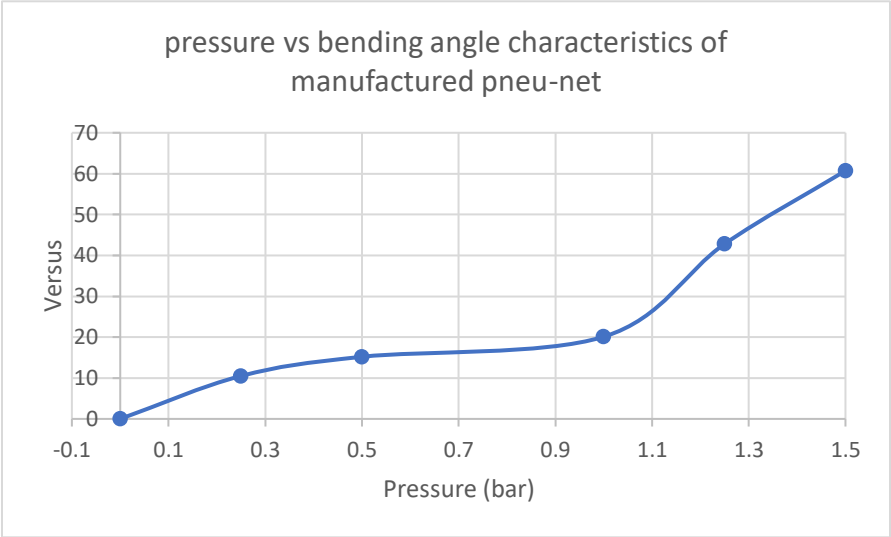

Figure A.6 (left) Testing setup for pressure versus bending angle characterization, (right) Pressure versus bending angle curve of the pneu-net actuator.

A.5. Discussion and shift to the next design

The first problem in this design lies in the integration of soft actuator and the flexible tube. Using flexible tube manufactured using Dragonskin 10, buckling happen (Figure A.7). This means when the actuator is activated, only one side will bend to the inside of the tube. Another tube alternative by gluing the actuator into flexible garden hose and washing machine hose are also tried. In both cases, the actuator bent inside the flexible tubes without flexing the outer tubes. The same thing happens with the previous tube: the actuator only bends inside without bending the entire tube structure. Another problem is the high pressure required to pressurize the actuator. To achieve 60^0 bending, the actuator needs 1.5 bar of pressure. This high pressure is riskier to damage the internal organ if leakage happens.

Considering the drawback of the first design, without being able to fulfil several important requirements, such as: safety of pressure applied, bendability of the entire structure, and bending angle of at least 90^0, we will pursue the next design, which build from previously tested STIFF-FLOP design.

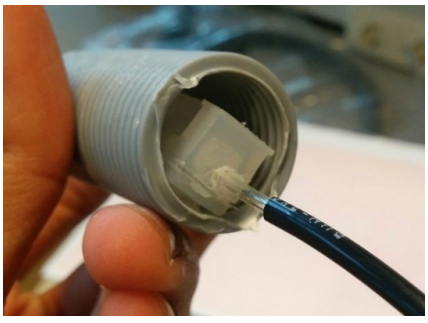

Figure A.7 (left) buckling of one side of actuator, (right) the actuator bends without bending the tube structure

B. List of material for MOLLUSC manipulator

Material:

1) Ecoflex 0050 Liquid Silicone Elastomer
2) Neoprene gloves
3) Fine coffee
4) Silicone glue
5) Silicone tubes with diameter of 2 mm
6) Tea bag
7) Parafilm
8) PET expandable braided sheath with maximum diameter of 25 mm
9) Thread